

# Octanuclear Heterobimetallic $\{\text{Ni}_4\text{Ln}_4\}$ Assemblies Possessing $\text{Ln}_4$ Square Grid $[2 \times 2]$ Motifs: Synthesis, Structure, and Magnetism

Sourav Biswas,<sup>†</sup> Joydeb Goura,<sup>†</sup> Sourav Das,<sup>‡</sup> Craig V. Topping,<sup>§</sup> Jamie Brambleby,<sup>||</sup> Paul A. Goddard,<sup>\*,||</sup> and Vadapalli Chandrasekhar<sup>\*,†,⊥</sup>

<sup>†</sup>Department of Chemistry, Indian Institute of Technology Kanpur, Kanpur-208016, India

<sup>‡</sup>Department of Chemistry, Institute of Infrastructure Technology Research and Management, Near Khokhara Circle, Maninagar East, Ahmedabad-380026, India

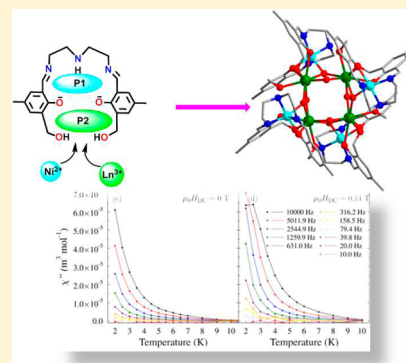
<sup>§</sup>Clarendon Laboratory, University of Oxford, Parks Road, Oxford, OX1 3PU, United Kingdom

<sup>||</sup>Department of Physics, University of Warwick, Gibbet Hill Road, Coventry, CV4 7AL, United Kingdom

<sup>⊥</sup>National Institute of Science Education and Research, Institute of Physics Campus, Sachivalaya Marg, PO: Sainik School, Bhubaneswar - 751 005, Orissa, India

## Supporting Information

**ABSTRACT:** Octanuclear heterobimetallic complexes,  $[\text{Ln}_4\text{Ni}_4(\text{H}_3\text{L})_4(\mu_3\text{-OH})_4(\mu_2\text{-OH})_4]4\text{Cl}\cdot x\text{H}_2\text{O}\cdot y\text{CHCl}_3$  ( $\text{Dy}^{3+}$ ,  $x = 30.6$ ,  $y = 2$  (1);  $\text{Tb}^{3+}$ ,  $x = 28$ ,  $y = 0$  (2);  $\text{Gd}^{3+}$ ,  $x = 25.3$ ,  $y = 0$  (3);  $\text{Ho}^{3+}$ ,  $x = 30.6$ ,  $y = 3$  (4)) ( $\text{H}_3\text{L} = \text{N}_1, \text{N}_3$ -bis(6-formyl-2-(hydroxymethyl)-4-methylphenol)diethylenetriamine) are reported. These are assembled by the cumulative coordination action of four doubly deprotonated compartmental ligands,  $[\text{H}_3\text{L}]^{2-}$ , along with eight exogenous  $-\text{OH}$  ligands. Within the core of these complexes, four  $\text{Ln}^{3+}$ 's are distributed to the four corners of a perfect square grid while four  $\text{Ni}^{2+}$ 's are projected away from the plane of the  $\text{Ln}_4$  unit. Each of the four  $\text{Ni}^{2+}$ 's possesses distorted octahedral geometry while all of the  $\text{Ln}^{3+}$ 's are crystallographically equivalent and are present in an elongated square antiprism geometry. The magnetic properties of compound 3 are dominated by an easy-plane single-ion anisotropy of the  $\text{Ni}^{2+}$  ions [ $D_{\text{Ni}} = 6.7(7)$  K] and dipolar interactions between  $\text{Gd}^{3+}$  centers. Detailed ac magnetometry reveals the presence of distinct temperature-dependent out-of-phase signals for compounds 1 and 2, indicative of slow magnetic relaxation. Magnetochemical analysis of complex 1 implies the 3d and the 4f metal ions are engaged in ferromagnetic interactions with SMM behavior, while dc magnetometry of compound 2 is suggestive of an antiferromagnetic Ni–Tb spin-exchange with slow magnetic relaxation due to a field-induced level crossing. Compound 4 exhibits an easy-plane single-ion anisotropy for the  $\text{Ho}^{3+}$  ions and weak interactions between spin centers.



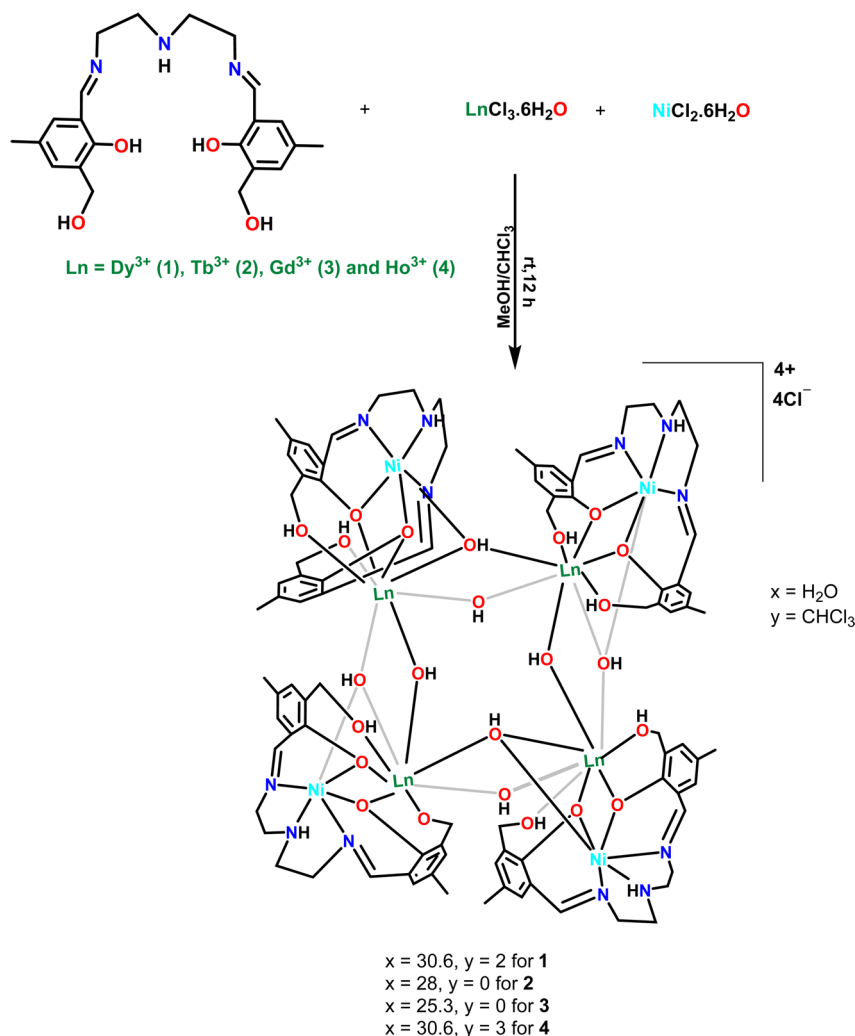
## INTRODUCTION

The discovery of single molecule magnet (SMM) behavior in  $[\text{Mn}^{\text{IV}}_4\text{Mn}^{\text{III}}_8(\mu_3\text{-O})_{12}(\text{CH}_3\text{CO}_2)_{16}(\text{OH}_2)_4]\cdot 2\text{MeCO}_2\text{H}\cdot 4\text{H}_2\text{O}$  has sparked enormous interest in the molecular complexes that can function as molecular magnets.<sup>1</sup> Apart from academic interest, SMMs also possess potential applications in various fields including quantum computing,<sup>2</sup> spintronics,<sup>3</sup> molecular storage devices,<sup>4</sup> etc. SMM properties are reflected by a frequency-dependent blocking temperature ( $T_B$ ), below which the system develops slow relaxation of magnetization with an effective energy barrier ( $U_{\text{eff}}$ ) preventing rapid reversal of the SMM magnetic moment. In general, the magnitude of the latter is influenced by (i) a high ground state spin ( $S$ ) and (ii) an Ising-type magnetic anisotropy ( $D < 0$ ).<sup>5</sup> Many of the initial synthetic efforts in this field were focused on polynuclear transition metal complexes, particularly those involving  $\text{Mn}^{\text{III}}$ .<sup>6</sup> The realization that a high  $S$  and  $D$  can also be obtained from other systems has turned attention toward homonuclear lanthanide complexes<sup>7</sup> as well as heterometallic 3d/4f

complexes.<sup>8</sup> Interest in the latter stems from two important reasons: (i) the 4f metal ions (particularly  $\text{Dy}^{3+}$ ,  $\text{Tb}^{3+}$ ,  $\text{Ho}^{3+}$ , and  $\text{Er}^{3+}$ ) exhibit a large magnetic anisotropy as result of unquenched spin–orbit coupling and possess a high spin, both of these factors contributing to promote a high  $U_{\text{eff}}$ ; (ii) unlike in homometallic 4f complexes where exchange coupling is very weak unless promoted by a radical ligand,<sup>9</sup> in 3d–4f complexes, effective exchange coupling between the 3d and heavy lanthanide centers seems to be possible. This not only stabilizes the bistable ground state but also to some extent suppresses quantum tunneling,<sup>10</sup> a mechanism that can bypass SMM behavior and provide fast magnetization relaxation. On the basis of these considerations, several 3d–4f heterometallic systems, notably, Cr–Ln,<sup>11</sup> Mn–Ln,<sup>12</sup> Fe–Ln,<sup>13</sup> Co–Ln,<sup>14</sup> Cu–Ln,<sup>15</sup> and Ni–Ln<sup>16</sup> (where Ln is a lanthanide ion), with varying nuclearities have been studied. Among these, Ni/Ln

Received: April 24, 2016

Published: August 8, 2016

Scheme 1. Schematic Depiction of the Syntheses of the Octanuclear  $Ni_4Ln_4$  Complexes 1–4

compounds are gaining unabated attention in view of their intriguing structural topologies as well as interesting SMM properties, essentially originating from second order angular momentum.<sup>16</sup> We have been working for some time on assembling new families of Ni–Ln systems with a view to discover new synthetic methodologies that allow us to modulate the nuclearity and topology of these complexes as well as to study their magnetic properties.<sup>16b,c,d</sup> Thus, recently, we have assembled a series of pentanuclear  $Ni_2Ln_3$ <sup>16b</sup> and hexanuclear  $Ni_3Ln_3$ <sup>16d</sup> complexes. The  $Dy^{III}$  analogue of the former family behaved as an SMM with an energy barrier of 85 K, the highest known among the Ni–Ln compounds, thus far. Recently, we have reported  $[2 \times 2]$  square grid homometallic  $Ln_4$  ensembles ( $Ln = Dy^{3+}$ ,  $Tb^{3+}$ ,  $Gd^{3+}$ , and  $Er^{3+}$ ) by utilizing a multidentate flexible ligand, 6-(hydroxymethyl)-*N* [1-(pyridin-2-yl)ethylidene]picolinohydrazide.<sup>17</sup> We wanted to incorporate the  $Ln_4$  grid motif in a heterometallic system by choosing a different multisite coordination ligand. Accordingly, we designed a multidentate compartmental Schiff base ligand,  $N_{1,3}$ -bis(6-formyl-2-(hydroxymethyl)-4-methylphenol)-diethylenetriamine ( $H_3L$ ), which upon reaction with  $LnCl_3 \cdot 6H_2O$  ( $Ln = Dy^{3+}$ ,  $Tb^{3+}$ ,  $Gd^{3+}$ , and  $Ho^{3+}$ ) and  $NiCl_2 \cdot 6H_2O$  afforded octanuclear heterometallic compounds,  $[Ln_4Ni_4(H_3L)_4(\mu_3-OH)_4(\mu_2-OH)_4]4Cl \cdot xH_2O \cdot yCHCl_3$  ( $Dy^{3+}$ ,  $x = 30.6$ ,  $y = 2$ ;  $Tb^{3+}$ ,  $x = 28$ ,  $y = 0$ ;  $Gd^{3+}$ ,  $x = 25.3$ ,  $y = 0$ ;

$Ho^{3+}$ ,  $x = 30.6$ ,  $y = 3$ ; Scheme 1). The synthesis, structure, and magnetic properties of these compounds are discussed herein.

## EXPERIMENTAL SECTION

Solvents and other general reagents used in this work were purified according to standard procedures.<sup>18</sup> Diethylenetriamine, 2,6-bis-(hydroxymethyl)-4-methylphenol, activated manganese(IV) dioxide ( $MnO_2$ ),  $DyCl_3 \cdot 6H_2O$ ,  $TbCl_3 \cdot 6H_2O$ ,  $HoCl_3 \cdot 6H_2O$ , and  $GdCl_3 \cdot 6H_2O$  were obtained from Sigma-Aldrich Chemical Co. and were used as received. Sodium sulfate (anhydrous) and  $NiCl_2 \cdot 6H_2O$  were obtained from SD Fine Chemicals, Mumbai, India, and were used as such. 6-Formyl-2-(hydroxymethyl)-4-methylphenol was prepared according to a literature procedure.<sup>16c</sup>

**Instrumentation.** Melting points were measured using a JSGW melting point apparatus and are uncorrected. Infrared (IR) spectra were recorded as KBr pellets on a Bruker Vector 22 FT IR spectrophotometer operating at  $400\text{--}4000\text{ cm}^{-1}$ . Elemental analyses of the compounds were obtained from Thermoquest CE Instruments CHNS-O, EA/110 model. Electrospray ionization mass spectrometry (ESI-MS) was carried out on a Micromass Quattro II triple quadrupole mass spectrometer.  $^1H$  NMR spectra were recorded in  $CDCl_3$  solutions on a JEOL JNM LAMBDA 400 model spectrometer operating at 500.0 MHz. Chemical shifts are reported in parts per million (ppm) and are referenced with respect to internal tetramethylsilane ( $^1H$ ).

**Magnetic Measurements.** Alternating-current (ac) and direct-current (dc) susceptibility measurements were performed on

Table 1. Crystal Data and Structure Refinement Parameters of 1–4

|                                      | 1  | 2  | 3   | 4  |
|--------------------------------------|--|--|---|--|
| formula                              | C <sub>264</sub> H <sub>336</sub> Cl <sub>12</sub> Dy <sub>12</sub> N <sub>36</sub> Ni <sub>12</sub> O <sub>92</sub> | C <sub>88</sub> H <sub>104</sub> Cl <sub>4</sub> N <sub>12</sub> Ni <sub>4</sub> O <sub>40</sub> Tb <sub>4</sub> | C <sub>276</sub> H <sub>324</sub> Cl <sub>12</sub> Gd <sub>12</sub> N <sub>36</sub> Ni <sub>12</sub> O <sub>142</sub> | C <sub>88</sub> H <sub>108</sub> Cl <sub>4</sub> Ho <sub>4</sub> N <sub>12</sub> Ni <sub>4</sub> O <sub>60</sub> |
| g/mol                                | 8565.59  | 2982.15  | 9434.61   | 9734.65  |
| cryst syst                           | cubic  | cubic  | cubic   | cubic  |
| space group                          | I $\bar{4}$ 3d   | I $\bar{4}$ 3d   | I $\bar{4}$ 3d  | I $\bar{4}$ 3d   |
| a/Å                                  | 34.040(5)  | 34.080(5)  | 34.090(5)   | 34.057(5)  |
| $\alpha = \gamma = \beta$ (deg)      | 90.000   | 90.000   | 90.000  | 90.000   |
| V/Å <sup>3</sup>                     | 39443(17)  | 39583(6)   | 39617(17)   | 39502(17)  |
| Z                                    | 4  | 12   | 4   | 4  |
| $\rho_c$ /g cm <sup>-3</sup>         | 1.442  | 1.501  | 1.582   | 1.637  |
| $\mu$ /mm <sup>-1</sup>              | 2.948  | 2.826  | 2.699   | 3.101  |
| F(000)                               | 1.442  | 17712.0  | 18704.0   | 19264.0  |
| cryst size (mm <sup>3</sup> )        | 0.12 × 0.067 × 0.064   | 0.15 × 0.09 × 0.04   | 0.08 × 0.043 × 0.031  | 0.093 × 0.033 × 0.026  |
| $\theta$ range (deg)                 | 4.15 to 25.02  | 4.14 to 24.73  | 4.14 to 25.02   | 2.15 to 25.01  |
| limiting indices                     | -44 ≤ h ≤ 45<br>-45 ≤ k ≤ 32<br>-42 ≤ l ≤ 45   | -40 ≤ h ≤ 39<br>-39 ≤ k ≤ 40<br>-26 ≤ l ≤ 40   | -41 ≤ h ≤ 45<br>-45 ≤ k ≤ 31<br>-45 ≤ l ≤ 39  | -22 ≤ h ≤ 45<br>-42 ≤ k ≤ 45<br>-45 ≤ l ≤ 42   |
| reflns collected                     | 177134   | 134249   | 177303  | 173264   |
| ind reflns                           | 5798[R(int) = 0.1577]  | 5639[R(int) = 0.0593]  | 5822[R(int) = 0.0834]   | 5797 [R(int) = 0.1011]   |
| completeness to $\theta$ (%)         | 99.4%  | 99.3%  | 99%   | 99.4%  |
| refinement method                    | full-matrix least-squares on F <sup>2</sup>  | full-matrix least-squares on F <sup>2</sup>  | full-matrix least-squares on F <sup>2</sup>   | full-matrix least-squares on F <sup>2</sup>  |
| data/restraints/params               | 5798/5/336   | 5639/6/374   | 5822/29/382   | 5797/10/385  |
| goodness-of-fit on F <sup>2</sup>    | 1.061  | 1.031  | 1.066   | 1.072  |
| final R indices [I > 2 $\sigma$ (I)] | R <sub>1</sub> = 0.0360<br>wR <sub>2</sub> = 0.0804  | R <sub>1</sub> = 0.0266<br>wR <sub>2</sub> = 0.0687  | R <sub>1</sub> = 0.0338<br>wR <sub>2</sub> = 0.0898   | R <sub>1</sub> = 0.0359<br>wR <sub>2</sub> = 0.0902  |
| R indices (all data)                 | R <sub>1</sub> = 0.0493<br>wR <sub>2</sub> = 0.0853  | R <sub>1</sub> = 0.0290,<br>wR <sub>2</sub> = 0.0701   | R <sub>1</sub> = 0.0391<br>wR <sub>2</sub> = 0.0938   | R <sub>1</sub> = 0.0396<br>wR <sub>2</sub> = 0.0920  |
| CCDC number                          | 1474090  | 1474091  | 1474092   | 1474093  |

powdered samples of compounds 1–4 (described as Ni<sub>4</sub>Dy<sub>4</sub>, Ni<sub>4</sub>Tb<sub>4</sub>, Ni<sub>4</sub>Gd<sub>4</sub>, and Ni<sub>4</sub>Ho<sub>4</sub> in the magnetic properties section) with masses of 36.5, 20.0, 23.0, and 24.6 mg, respectively, dispersed in Vaseline in gelatin capsules to prevent powder movement during measurements.

Dc measurements were performed in a Quantum Design Magnetic Property Measurement System (MPMS XL) to determine both the molar susceptibility in dc fields  $\mu_0 H_{DC} = 0.1$  T ( $\chi_{mol} = M/nH_{DC}$ , where  $M$  is the magnetization and  $n$  the number of moles) for temperatures in the range  $1.8 \leq T \leq 300$  K and the isothermal magnetization up to a magnetic field of  $\mu_0 H_{DC} = 7$  T at 2.0 K.

Ac measurements of in-phase and out-of-phase susceptibilities,  $\chi'$  and  $\chi''$ , respectively, were performed using both a Quantum Design MPMS and a Quantum Design Physical Property Measurement System (PPMS). Ac fields with frequencies in the range of  $10 \leq \nu \leq 1000$  Hz (MPMS) and  $10 \leq \nu \leq 10000$  Hz (PPMS) and amplitudes  $0.1 \leq \mu_0 H_{AC} \leq 0.4$  mT were used, and measurements were performed for temperatures down to 2.0 K. Measurements of Ni<sub>4</sub>Gd<sub>4</sub> and Ni<sub>4</sub>Ho<sub>4</sub> were recorded for dc applied fields of  $\mu_0 H_{DC} = 0$  and 0.1 T, while the slow relaxation properties of Ni<sub>4</sub>Dy<sub>4</sub> and Ni<sub>4</sub>Tb<sub>4</sub> were explored for dc fields  $\leq 0.4$  T and  $\leq 0.7$  T, respectively. Wait times up to 45 s were included after changing the ac-field frequency to ensure reproducibility of the data.

**X-ray Crystallography.** The crystal data for the compounds have been collected on a Bruker SMART CCD diffractometer (Mo K $\alpha$  radiation,  $\lambda = 0.71073$  Å). The program SMART<sup>19a</sup> was used for collecting frames of data, indexing reflections, and determining lattice parameters; SAINT<sup>19a</sup> for integration of the intensity of reflections and scaling; SADABS<sup>19b</sup> for absorption correction; and SHELXL<sup>19c,d</sup> for space group and structure determination and least-squares refinements on F<sup>2</sup>. The crystal structures were solved and refined by full-matrix least-squares methods against F<sup>2</sup> by using the program SHELXL-2014<sup>19e</sup> using Olex-2 software.<sup>19f</sup> All the non-hydrogen atoms were refined with anisotropic displacement parameters. Hydrogen positions were fixed at calculated positions and refined isotropically. Some of the lattice solvent molecules of all the complexes cannot be modeled satisfactorily due to the presence of severe disorders. Therefore, the

Olex-2 mask program has been performed to discard those disordered solvent molecules and gave electron densities of 353.6, 120.15, 59.5, and 171.1 corresponding to the complexes 1, 2, 3, and 4, respectively. These can be tentatively assigned as 24H<sub>2</sub>O and 2CHCl<sub>3</sub> for 1, 12H<sub>2</sub>O for 2, 6H<sub>2</sub>O for 3, and 3CHCl<sub>3</sub> for 4. The crystallographic figures have been generated using Diamond 3.1e software.<sup>19g</sup> The crystal data and the cell parameters for compounds 1–4 are summarized in Table 1. Crystallographic data (excluding structure factors) for the structures in this paper have been deposited with the Cambridge Crystallographic Data Centre as supplementary publication nos. CCDC 1474090–1474093. Copies of the data can be obtained, free of charge, on application to CCDC, 12 Union Road, Cambridge CB2 1EZ, U.K., <http://www.ccdc.cam.ac.uk>, e-mail: [data\\_request@ccdc.cam.ac.uk](mailto:data_request@ccdc.cam.ac.uk) or fax: + 44 1223 336033.

**Synthesis.** N<sub>1</sub>,N<sub>3</sub>-Bis(6-formyl-2-(hydroxymethyl)-4-methylphenol)diethylenetriamine (H<sub>3</sub>L). An ethanolic solution (20 mL) of 6-formyl-2-(hydroxymethyl)-4-methylphenol (1.5 g, 8.94 mmol) was added dropwise to a vigorously stirred solution of diethylenetriamine (0.46 g, 4.47 mmol) over a period of 20 min in ethanol (80 mL) at room temperature. The resulting yellow colored solution was refluxed for 6 h. Subsequently, the solution was concentrated to 30 mL in vacuo before being kept in a refrigerator at 0 °C overnight. A yellow colored precipitate was obtained, which was filtered, washed with diethyl ether and cold methanol, and dried. Yield: 1.3 g (72.7%). M.P: 146 °C. FT-IR (KBr) cm<sup>-1</sup>: 3429 (br), 3277 (s), 2922 (m), 2854 (m), 1630 (s), 1603 (s), 1463 (m), 1371 (m), 1311 (w). <sup>1</sup>H NMR (500 MHz, CDCl<sub>3</sub>,  $\delta$ , ppm): 2.25 (s, 6H, Ar–Me), 2.98 (t, 4H, –CH<sub>2</sub>), 3.70 (t, 4H, –CH<sub>2</sub>), 4.65 (s, 2H, Ar–CH<sub>2</sub>OH), 6.95 (s, 1H, Ar–H), 7.11 (s, 1H, Ar–H), 8.31 (s, 1H, imine–H), 9.80 (b, H, –NH). Anal. Calcd for C<sub>22</sub>H<sub>29</sub>N<sub>3</sub>O<sub>4</sub> (399.48): C, 66.14; H, 7.32; N, 10.52. Found: C, 65.85; H, 7.18; N, 10.63. ESI-MS,  $m/z$ : (M+H)<sup>+</sup>, 400.22.

**General Synthetic Procedure for the Preparation of the Complexes 1–4.** All of the metal complexes (1–4) were synthesized by following the same procedure as follows. H<sub>3</sub>L (0.04 g, 0.1 mmol) was dissolved in a solution of MeOH/CHCl<sub>3</sub> (40 mL), and

subsequently  $\text{LnCl}_3 \cdot 6\text{H}_2\text{O}$  (0.1 mmol) was added, followed by the addition of triethylamine (0.02 g, 0.2 mmol). The resulting light yellow colored solution was stirred for 1 h. At this stage, methanolic solution (10 mL) of  $\text{NiCl}_2 \cdot 6\text{H}_2\text{O}$  (0.024 g, 0.1 mmol) was added, followed by the addition of a further two equivalents of triethylamine. The green–yellow-colored reaction mixture was stirred at room temperature overnight. The reaction mixture was stripped off the solvent in vacuo to afford a green residue which was washed twice with diethyl ether and dried and dissolved in a 1:1 v/v mixture of methanol and chloroform. Dark green colored crystals, which were suitable for X-ray diffraction, were obtained by a slow evaporation of the solvent mixture for about 10 days. Specific details of each reaction and the characterization data of the compounds are outlined below.

$[\text{Dy}_4\text{Ni}_4(\text{H}_3\text{L})_4(\mu_3\text{-OH})_4(\mu_2\text{-OH})_4]4\text{Cl} \cdot 30.6\text{H}_2\text{O} \cdot 2\text{CHCl}_3$  (**1**). Quantities:  $\text{H}_3\text{L}$  (0.04 g, 0.1 mmol),  $\text{DyCl}_3 \cdot 6\text{H}_2\text{O}$  (0.038 g, 0.1 mmol),  $\text{Et}_3\text{N}$  (0.052 mL, 0.4 mmol). Yield: 0.039 g, 43.8% (based on  $\text{Dy}^{3+}$ ). M.P:  $260 > ^\circ\text{C}$ . FT-IR (KBr)  $\text{cm}^{-1}$ : 3436 (br), 2932 (br), 2870 (s), 1641 (s), 1568 (s), 1460 (s), 1451 (s), 1393 (s), 1336 (w), 1301 (w), 1263 (s), 1234 (s), 1107 (w), 1087 (m), 960 (m), 923 (m), 874 (w), 812 (w), 710 (w). ESI-MS  $m/z$ , ion: 1340.6,  $[\text{C}_{88}\text{H}_{116}\text{Dy}_4\text{Ni}_4\text{O}_{24} + \text{MeOH} + \text{MeCN} - 2\text{H}^+]^{2+}$ . Anal. Calcd for  $\text{C}_{90}\text{H}_{175.2}\text{Dy}_4\text{Ni}_4\text{O}_{54.6}\text{Cl}_{10}$  (3538.50): C, 30.55; H, 4.99; N, 4.75. Found: C, 31.48; H, 4.57; N, 5.34.

$[\text{Tb}_4\text{Ni}_4(\text{H}_3\text{L})_4(\mu_3\text{-OH})_4(\mu_2\text{-OH})_4]4\text{Cl} \cdot 28\text{H}_2\text{O}$  (**2**). Quantities:  $\text{H}_3\text{L}$  (0.04 g, 0.1 mmol),  $\text{TbCl}_3 \cdot 6\text{H}_2\text{O}$  (0.037 g, 0.1 mmol),  $\text{Et}_3\text{N}$  (0.052 mL, 0.4 mmol). Yield: 0.029 g, 39.1% (based on  $\text{Tb}^{3+}$ ). M.P:  $260 > ^\circ\text{C}$ . FT-IR (KBr)  $\text{cm}^{-1}$ : 3422 (br), 2932 (br), 2874 (s), 1643 (s), 1564 (s), 1465 (s), 1447 (s), 1393 (s), 1328 (w), 1298 (w), 1257 (s), 1233 (s), 1108 (w), 1081 (m), 963 (m), 925 (m), 869 (w), 811 (w), 709 (w). ESI-MS  $m/z$ , ion: 1360.11,  $[\text{C}_{88}\text{H}_{116}\text{Tb}_4\text{Ni}_4\text{O}_{24} + 7\text{H}_2\text{O} - 2\text{H}^+]^{2+}$ . Anal. Calcd for  $\text{C}_{88}\text{H}_{120}\text{Cl}_4\text{Ni}_4\text{O}_{40}\text{Tb}_4$  (2992.09): C, 35.25; H, 4.03; N, 5.61. Found: C, 35.93; H, 3.89; N, 5.27.

$[\text{Gd}_4\text{Ni}_4(\text{H}_3\text{L})_4(\mu_3\text{-OH})_4(\mu_2\text{-OH})_4]4\text{Cl} \cdot 25.3\text{H}_2\text{O}$  (**3**). Quantities:  $\text{H}_3\text{L}$  (0.04 g, 0.1 mmol),  $\text{GdCl}_3 \cdot 6\text{H}_2\text{O}$  (0.037 g, 0.1 mmol),  $\text{Et}_3\text{N}$  (0.052 mL, 0.4 mmol). Yield: 0.027 g, 34.1% (based on  $\text{Gd}^{3+}$ ). M.P:  $260 > ^\circ\text{C}$ . FT-IR (KBr)  $\text{cm}^{-1}$ : 3422 (br), 2937 (br), 2867 (s), 1641 (s), 1569 (s), 1461 (s), 1450 (s), 1393 (s), 1332 (w), 1303 (w), 1255 (s), 1238 (s), 1109 (w), 1081 (m), 965 (m), 922 (m), 863 (w), 811 (w), 708 (w). ESI-MS  $m/z$ , ion: 1343.59,  $[\text{C}_{88}\text{H}_{116}\text{Gd}_4\text{Ni}_4\text{O}_{24} + \text{MeCN} + \text{H}_2\text{O} - 2\text{H}^+]^{2+}$ . Anal. Calcd for  $\text{C}_{88}\text{H}_{158.6}\text{Gd}_4\text{Ni}_4\text{O}_{49.3}\text{Cl}_4$  (3179.23): C, 33.25; H, 5.03; N, 5.29. Found: C, 33.89; H, 4.93; N, 5.02.

$[\text{Ho}_4\text{Ni}_4(\text{H}_3\text{L})_4(\mu_3\text{-OH})_4(\mu_2\text{-OH})_4]4\text{Cl} \cdot 36\text{H}_2\text{O} \cdot 3\text{CHCl}_3$  (**4**). Quantities:  $\text{H}_3\text{L}$  (0.04 g, 0.1 mmol),  $\text{HoCl}_3 \cdot 6\text{H}_2\text{O}$  (0.038 g, 0.1 mmol),  $\text{Et}_3\text{N}$  (0.052 mL, 0.4 mmol). Yield: 0.036 g, 39.3% (based on  $\text{Ho}^{3+}$ ). M.P:  $260 > ^\circ\text{C}$ . FT-IR (KBr)  $\text{cm}^{-1}$ : 3429 (br), 2935 (br), 2871 (s), 1645 (s), 1563 (s), 1465 (s), 1451 (s), 1397 (s), 1332 (w), 1304 (w), 1260 (s), 1239 (s), 1105 (w), 1082 (m), 967 (m), 929 (m), 871 (w), 814 (w), 711 (w). ESI-MS  $m/z$ , ion: 1345.11,  $[\text{C}_{88}\text{H}_{116}\text{Ho}_4\text{Ni}_4\text{O}_{24} + 4\text{H}_2\text{O} - 2\text{H}^+]^{2+}$ . Anal. Calcd for  $\text{C}_{91}\text{H}_{169.2}\text{Ho}_4\text{Ni}_4\text{O}_{54.6}\text{Cl}_{13}$  (3660.54): C, 29.86; H, 4.66; N, 4.59. Found: C, 29.33; H, 5.01; N, 5.12.

## RESULTS AND DISCUSSION

**Synthetic Aspects.** In designing ligands for the preparation of heterometallic 3d/4f complexes, the following key factors must be kept in mind.<sup>16</sup> Distinct coordination compartments are needed within the ligand coordination sphere so as to selectively bind simultaneously to transition metal ions and lanthanide metal ions. In addition, the ligand should be able to promote efficient exchange interaction between the two types of metal centers. Many ligands are known in the literature that have served this purpose.<sup>15,16</sup> In 2014, Tang et al. reported a series of defect-dicubane-shaped  $\text{Ni}_4\text{Ln}_2$  ( $\text{Ln} = \text{Dy}^{3+}$ ,  $\text{Tb}^{3+}$ ,  $\text{Ho}^{3+}$ ,  $\text{Gd}^{3+}$ , and  $\text{Y}^{3+}$ ; Figure 1) complexes by employing a compartmental ligand,  $N_1, N_3$ -bis(3-methoxysalicylidene) diethylenetriamine.<sup>20f</sup>

Considering that the flexible nature of the  $-\text{CH}_2\text{OH}$  motif allows it to adapt to the coordination requirements of the various metal ions, in polynuclear complexes, much better than

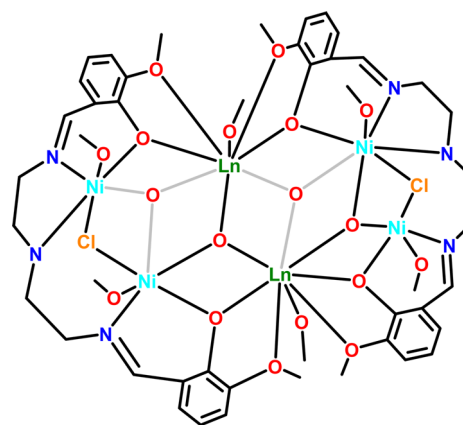
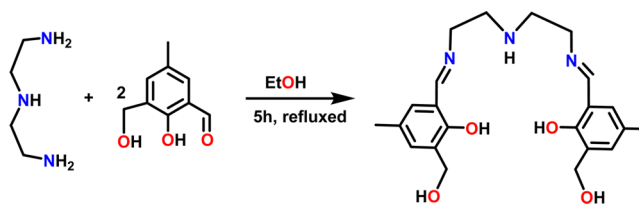


Figure 1. Defect-dicubane-shaped  $\text{Ni}_4\text{Ln}_2$ .<sup>20f</sup>

the  $-\text{OMe}$  group, we modified Tang's ligand to prepare  $\text{H}_3\text{L}$  by the condensation of 6-formyl-2-(hydroxymethyl)-4-methylphenol with diethylenetriamine ( $\text{H}_3\text{L}$ ; Scheme 2).

### Scheme 2. Synthesis of Ligand $\text{H}_3\text{L}$



In its doubly deprotonated form,  $[\text{H}_3\text{L}]^{2-}$  is partitioned into two compartments: one of them is pentadentate, having a  $\text{N}_3\text{O}_2$  environment which is suitable to hold 3d metal ions, whereas the other compartment is tetradentate, comprised of an  $\text{O}_4$  environment, and is expected to bind to oxophilic lanthanide metal ions (Figure 2a). In accordance with the above

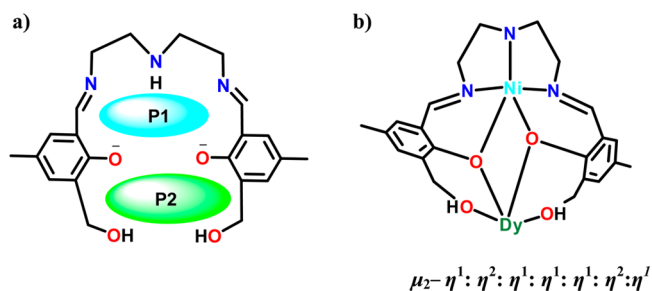
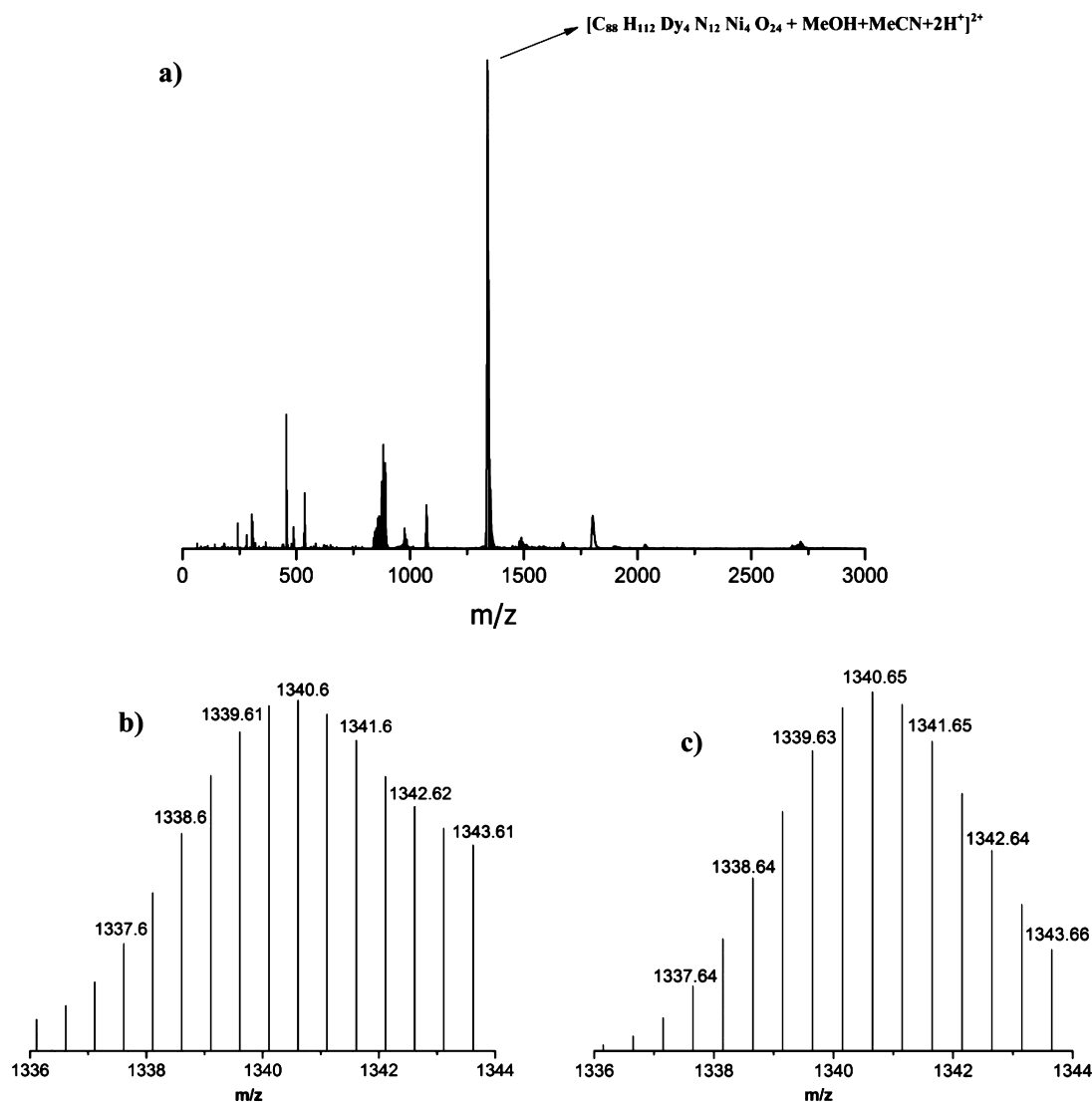


Figure 2. (a) The two distinct coordination compartments in  $[\text{H}_3\text{L}]^{2-}$ . (b) coordination mode of  $[\text{H}_3\text{L}]^{2-}$  in **1**.

expectations, the sequential reaction of  $\text{H}_3\text{L}$  with the  $\text{LnCl}_3 \cdot 6\text{H}_2\text{O}$  and  $\text{NiCl}_2 \cdot 6\text{H}_2\text{O}$  followed by the addition of triethylamine in a stoichiometric ratio of 1:1:1:5 in methanol/chloroform mixture (1:1 v/v) has afforded a series of tetracationic octanuclear heterometallic complexes,  $[\text{Ln}_4\text{Ni}_4(\text{H}_3\text{L})_4(\mu_3\text{-OH})_4(\mu_2\text{-OH})_4]4\text{Cl} \cdot x\text{H}_2\text{O} \cdot y\text{CHCl}_3$  ( $\text{Dy}^{3+}$ ,  $x = 30.6$ ,  $y = 2$ ;  $\text{Tb}^{3+}$ ,  $x = 28$ ,  $y = 0$ ;  $\text{Gd}^{3+}$ ,  $x = 25.3$ ,  $y = 0$ ;  $\text{Ho}^{3+}$ ,  $x = 30.6$ ,  $y = 3$ ; Scheme 1). The molecular structures of complexes **1–4** were determined by X-ray crystallography.

To investigate the structural integrity of **1–4** in solution, we have carried out ESI-MS studies which revealed peaks at mass to charge ratios of 1340.6, 1360.11, 1343.59, and 1345.11



**Figure 3.** (a) Full range ESI-MS spectrum of complex **1**. (b) Experimental and (c) simulated mass spectral pattern of the species  $[\text{C}_{88}\text{H}_{116}\text{Dy}_4\text{N}_{12}\text{Ni}_4\text{O}_{24} + \text{MeOH} + \text{MeCN} - 2\text{H}^+]^{2+}$ .

corresponding to the dicationic species  $[\text{C}_{88}\text{H}_{116}\text{Dy}_4\text{N}_{12}\text{Ni}_4\text{O}_{24} + \text{MeOH} + \text{MeCN} - 2\text{H}^+]^{2+}$ ,  $[\text{C}_{88}\text{H}_{116}\text{Tb}_4\text{N}_{12}\text{Ni}_4\text{O}_{24} + 7\text{H}_2\text{O} - 2\text{H}^+]^{2+}$ ,  $[\text{C}_{88}\text{H}_{116}\text{Gd}_4\text{N}_{12}\text{Ni}_4\text{O}_{24} + \text{MeCN} + \text{H}_2\text{O} - 2\text{H}^+]^{2+}$ , and  $[\text{C}_{88}\text{H}_{116}\text{Ho}_4\text{N}_{12}\text{Ni}_4\text{O}_{24} + 4\text{H}_2\text{O} - 2\text{H}^+]^{2+}$ , respectively. These results suggest that, overall, the octanuclear motifs seem to survive in solution. The ESI-MS spectrum of **1** is shown in Figure 3, while those of **2–4** are given in the Supporting Information (Figures S1–S3).

**X-ray Crystal Structures of 1–4.** Crystals suitable for X-ray analysis were obtained over a week by slow evaporation of solutions (1:1 (v/v) mixture of chloroform and methanol) of the corresponding complexes. Single-crystal X-ray diffraction analysis reveals that all four complexes are tetracationic and isostructural and crystallize in a cubic system in the space group  $I\bar{4}3d$  with two different *Z* values: *Z* = 4 for **1**, **3**, and **4** while *Z* = 12 for **2**. The asymmetric unit of **1–4** contains one-fourth of the total molecule, viz.,  $[\text{Ni}^{\text{II}}\text{Ln}^{\text{III}}(\text{H}_3\text{L})(\mu_2\text{-OH})(\text{OH})]\text{Cl}$  (Figure 4a), and the full molecule is generated by the 4-fold axis of rotation ( $C_4$ ), which passes exactly through the center of the molecule (Figure 4b). In view of their structural similarity, complex **1** has been chosen as a representative example to elucidate the salient structural features. A perspective view of

the molecular structure of **1** is depicted in Figure 4b, while those of **2–4** are given in the Supporting Information.

Detailed structural analysis reveals that the octanuclear heterometallic complex **1** is assembled by the cumulative coordination action of four doubly deprotonated ligands,  $[\text{H}_3\text{L}]^{2-}$ . Each  $[\text{H}_3\text{L}]^{2-}$  holds two different metal ions:  $\text{Ni}^{\text{II}}$  occupies the P1 pocket ( $\text{N}_3\text{O}_2$ ), whereas the oxophilic  $\text{Dy}^{\text{III}}$  is held by the P2 pocket (O4; Figure 2a).  $\text{Ni}^{\text{II}}$  and  $\text{Dy}^{\text{III}}$  are connected by two bridging phenolate oxygen centers along with an exogenous  $\mu_3$ -OH ligand, giving rise to a dinuclear subunit,  $[\text{NiDy}(\text{H}_3\text{L})(\mu_3\text{-OH})]$ . Within this dinuclear subunit, each  $[\text{H}_3\text{L}]^{2-}$  adopts a  $\mu_2\text{-}\eta^1\text{:}\eta^2\text{:}\eta^1\text{:}\eta^1\text{:}\eta^1\text{:}\eta^2\text{:}\eta^1$  coordination mode to hold the two metal centers simultaneously (Figure 2b). In addition to the binding provided by  $[\text{H}_3\text{L}]^{2-}$ , four such  $\{\text{NiDy}\}$  subunits are tightly held together by four exogenous  $\mu_2$ -OH ligands to furnish finally an octanuclear heterometallic complex. The assignment of the protonation on the oxygen centers has been confirmed by BVS calculation<sup>21</sup> (Table 2).

The tetracationic octanuclear core,  $[\text{Dy}_4\text{Ni}_4(\mu_2\text{-O}_{\text{phen}})_8(\mu_2\text{-OH})_4(\mu_3\text{-OH})_4]^{4+}$ , comprises four dysprosium centers, which are arranged in the four corners of a square grid while the four  $\text{Ni}^{\text{II}}$  are displaced by  $\sim 2.3$  Å on either side of the  $\text{Dy}_4$  square

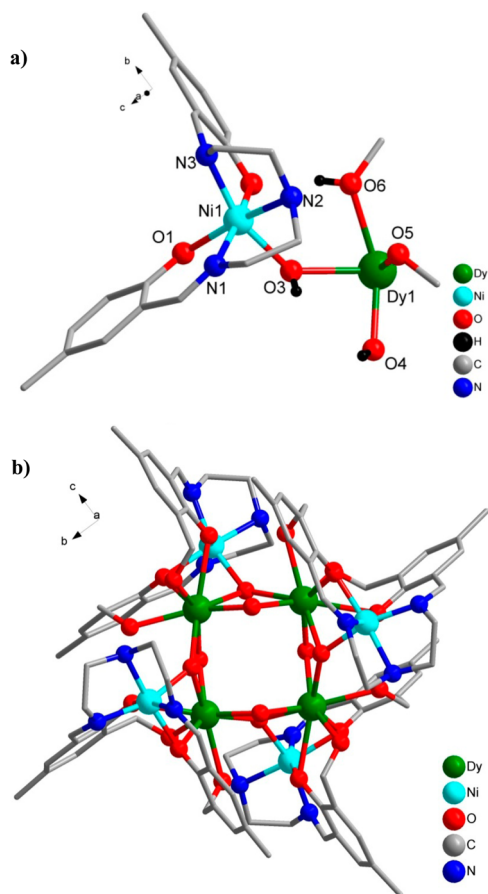


**Figure 4.** (a) Asymmetric unit of **1**. (b) Molecular structure of **1** (hydrogen atoms, chlorides, and solvent molecules are omitted for clarity). Selected bond lengths (Å) and bond angles(deg) are as follows: Ni(1)–N(3) = 2.009(11), Ni(1)–N(1) = 2.040(10), Ni(1)–O(1) = 2.088(8), Ni(1)–O(3) = 2.089(8), Ni(1)–O(2) = 2.097(8), Ni(1)–N(2) = 2.166(11), Ni(1)–Dy(1)\* = 3.2138(15), Dy(1)–O(4) = 2.211(7), Dy(1)–O(4)\* = 2.267(7), Dy(1)–O(1)\* = 2.364(7), Dy(1)–O(3)\* = 2.381(7), Dy(1)–O(5) = 2.420(8), Dy(1)–O(6) = 2.456(8), Dy(1)–O(2)\* = 2.631(8), Dy(1)–Ni(1)\* = 3.213(15), Ni(1)–O(1)–Dy(1)\* = 92.2(3), Ni(1)–O(2)–Dy(1)\* = 84.8(3), Ni(1)–OH(3)–Dy(1)\* = 91.7(3), Ni(1)–O(3)–Dy(1) = 139.7(4), Dy(1)\*–OH(3)–Dy(1) = 102.0(3), Dy(1)–OH(4)–Dy(1)\* = 113.3(3), Ni(1)\*–Dy(1)–Dy(1)\* = 127.90(4), Ni(1)\*–Dy(1)–Dy(1)\* = 74.88(3).

**Table 2.** Atom BVS Assignment

| atom | value | assigned as         |
|------|-------|---------------------|
| O3   | 1.08  | –OH                 |
| O4   | 1.18  | –OH                 |
| O6   | 0.402 | –CH <sub>2</sub> OH |

grid plane (Figure 5a). An interesting feature of the molecular structure of **1** is that all four dysprosium centers are coplanar, having an equal Dy–Dy distance of 3.74 Å resulting in a perfect [2 × 2] square grid (Figure 5b). It is of interest to mention that this kind of structural topology is quite rare in the 3d/4f complexes with only one reported in the Cr/Ln family.<sup>11c</sup> However, among homometallic lanthanide complexes, four examples are known that possess distorted square grid cores.<sup>17,22</sup>

The four Ni<sup>II</sup> ions in **1** are equivalent and are surrounded by a N<sub>3</sub>O<sub>3</sub> coordination environment. Each Ni<sup>II</sup> possesses a

distorted *fac* octahedral geometry; the three corners of one face are occupied by the nitrogen atoms. Two corners of the opposite face are from the phenoxo group, while the remaining is occupied by an oxygen belonging to a μ<sub>3</sub>-OH (Figure 6a).

Each of the four Dy<sup>III</sup>s is eight-coordinated in a distorted square antiprism geometry, the coordination environment being entirely made up of oxygen centers, which include two phenoxo oxygen atoms, two pendant –CH<sub>2</sub>OH, two μ<sub>3</sub>-OH, and two μ<sub>2</sub>-OH (Figure 6b). As anticipated, the flexible nature of the –CH<sub>2</sub>OH motif results in expansion of the nuclearity up to eight. In order to determine the amount of distortion present in the SAP geometry around Dy<sup>3+</sup>, we have calculated the skew angle ( $\varphi$ ), interplanar distances ( $d_{pp}$ ), intraplanar distance ( $d_{ip}$ ), and the dihedral angle between the two mean planes ( $\theta$ ) coming from the neighboring ligand donor sites and the angle between the S8 axis and a Ln–L direction ( $\alpha$ ; Table 3).<sup>23</sup>

The analysis of the above data reveals that the geometry around Dy<sup>III</sup> substantially deviates from the ideal SAP and can be best assigned as an elongated square antiprism geometry.

A few comments on the metric parameters observed in **1**. All the Ni–N bond distances are found to be almost similar to values in the range 1.996–2.047 Å. The Ni–O bond distances are nearly similar and fall in a narrow range, 2.071–2.111 Å, while the Dy–O bond distances fall in a wider range, 2.371–2.634 Å, with the largest distance being found in Dy–O<sub>phenolate</sub>. The average Dy–μ<sub>3</sub>-OH bond distance is 2.408 Å, which is larger than the average Dy–μ<sub>2</sub>-OH bond distance, 2.240 Å. These distances are similar to those observed in the literature.<sup>24</sup> All the Dy–μ<sub>3</sub>-OH–Dy bond angles are equal (101.93°) and are smaller than the Dy–μ<sub>2</sub>-OH–Dy bond angle, 113.23°. Three different Dy–O–Ni bond angles are found in compound **1**: the angles 84.75° and 92.47° correspond to two Dy–O<sub>phenolate</sub>–Ni angles, while 90.95° corresponds to Dy–μ<sub>3</sub>-OH–Ni.

The analysis of the packing arrangement of **1** shows a lack of significant intermolecular interactions among the neighboring molecules in any direction (Figures S7–S9); however, three sets of strong intramolecular hydrogen bonding are encountered: In one type, four hydrogen bonds are formed between the four pendant –CH<sub>2</sub>OH's of the [H<sub>3</sub>L]<sup>2-</sup> and the bridging phenolate oxygen atom of the four adjacent [H<sub>3</sub>L]<sup>2-</sup>s with D–H...A, 1.866 Å (Figure S10). Presumably, because of this interaction, the pendant –CH<sub>2</sub>OH is reluctant to undergo deprotonation to function as a bridging ligand and fails to expand the nuclearity further. In another type of hydrogen bonding, two chloride counteranions (Cl1 and Cl1\*) are involved in the formation of four intramolecular hydrogen bonds each among the two μ<sub>2</sub>-OH's and two μ<sub>3</sub>-OH's. The last type of hydrogen bonding involves two hydrogen atoms of the two ethylene arms of the [H<sub>3</sub>L]<sup>2-</sup>, which participate in hydrogen bonding with the remaining two chloride counteranions (Cl3 and Cl3\*; Figure S10). The hydrogen bond parameters involved in these various interactions are tabulated in Table 4. It is of interest to mention that as a result of the above-mentioned hydrogen bonding, four chloride counteranions are placed in a single straight line which passes exactly through the center of the molecule (Figure S10).

The geometry of the Ni<sub>4</sub>Ln<sub>4</sub> in the present work is unique; a literature search on Ni–Ln complexes reveals that only one octanuclear heterometallic Ni<sub>4</sub>Ln<sub>4</sub> complex is known so far,<sup>25</sup> possessing a completely different topology from the present case (Figure 7).

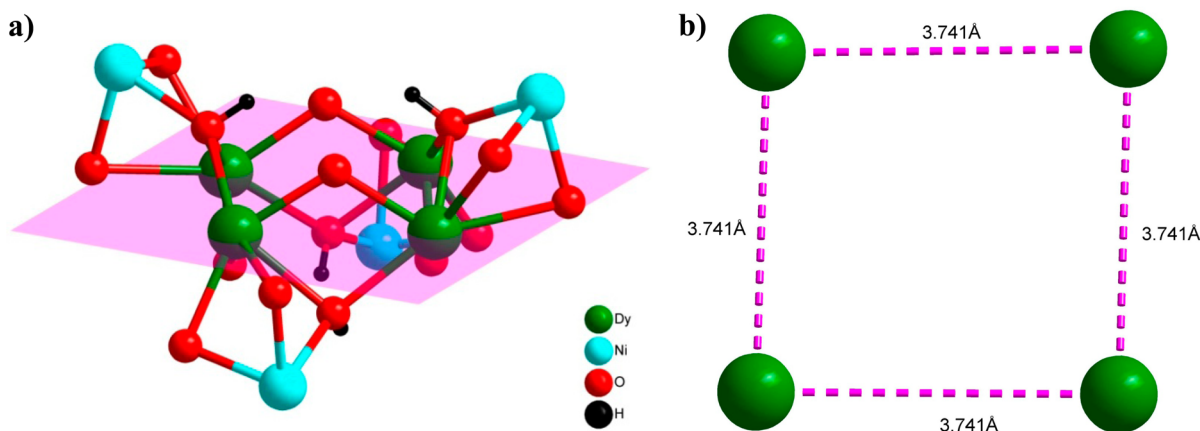


**Figure 5.** (a) Octanuclear core of complex **1** showing the coplanar arrangement of the Dy<sup>3+</sup> ions (shaded pink). (b) [2 × 2] square grid showing identical distances between nearest neighbor Dy<sup>3+</sup> ions.

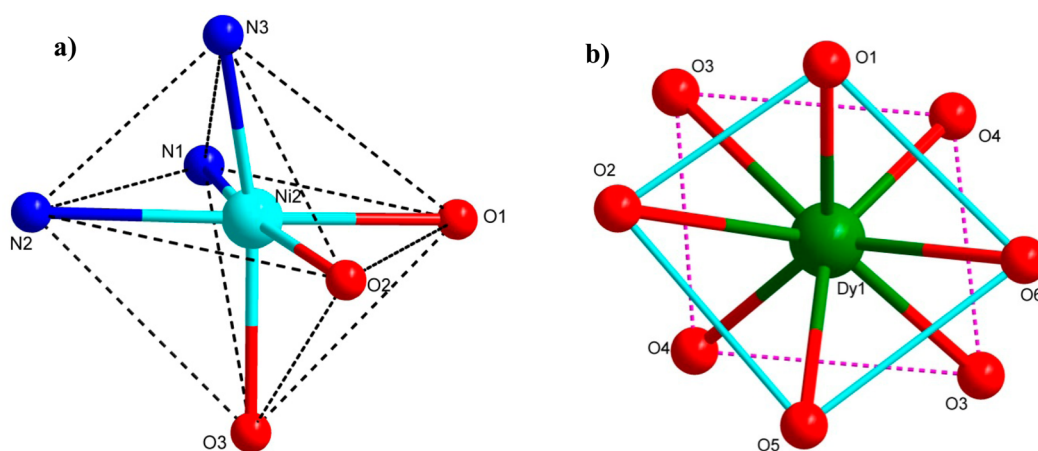


**Figure 6.** (a) Distorted octahedral geometry around the Ni<sup>2+</sup>. (b) Distorted square antiprism geometry around the Dy<sup>3+</sup>.

**Table 3. Parameters Involved in SAP Geometry for Compound 1 Compared to the Ideal Geometry**

| parameters | present case | ideal SAP         |
|------------|--------------|-------------------|
| $\varphi$  | 50.693°      | 45°               |
| $d_{pp}$   | 2.591 Å      | $d_{pp} = d_{ip}$ |
| $d_{ip}$   | 2.845 Å      |                   |
| $\theta$   | 1.438°       | 0°                |
| $\alpha$   | 53.318°      | 54.74             |

However, as we mentioned earlier, four Dy<sub>4</sub> complexes are reported with a distorted [2 × 2] square grid core topology<sup>17,22</sup> (Figure 8); among them two are similar to the Ln<sub>4</sub> motif of the present case.<sup>17,22c</sup> A comparison of the metric parameters of these reported complexes with those observed in the present instance is given in Table 5. From this table, it can be seen that the metric parameters involved are quite similar, most remarkable being the similarity of the inter Dy–Dy distances.

**Table 4. Intramolecular Hydrogen Bonding Parameters for Compound 1**

| D–H...A        | $d(D-H)$ (Å) | $d(H...A)$ (Å) | $d(D...A)$ (Å) | $\angle(DHA)$ (deg) | symmetry of A                 |
|----------------|--------------|----------------|----------------|---------------------|-------------------------------|
| O6–H6...O2     | 0.850        | 1.866          | 2.709(88)      | 171.3               | 1.25 – x, –0.75 + z, 0.75 – y |
| C12–H12A...Cl3 | 0.971        | 2.879          | 3.836(14)      | 168.3               | 1.5 – x, –y, 0.5 + z          |
| O3–H60...Cl1   | 0.914        | 2.516          | 3.314(64)      | 146                 | 1.5 – x, –y, 0.5 + z          |
| O4–H20...Cl1   | 0.831        | 2.578          | 3.252(50)      | 138.5               | 1.5 – x, –y, 0.5 + z          |

**Magnetic Studies.** To estimate which of the spin-exchange interactions we expect to dominate in compounds **1–4** (described in what follows as Ni<sub>4</sub>Dy<sub>4</sub>, Ni<sub>4</sub>Tb<sub>4</sub>, Ni<sub>4</sub>Gd<sub>4</sub>, and Ni<sub>4</sub>Ho<sub>4</sub>), we examine the potential magnetic pathways in the Ni<sub>4</sub>Ln<sub>4</sub> clusters (Figure 9). Of the three unique inter-ion magnetic exchanges, Ni–Ni, Ni–Ln, and Ln–Ln, the Ni–Ni interaction may be dismissed due to the lack of a clear superexchange pathway between Ni<sup>2+</sup> ions. Thus, we represent the clusters with a Hamiltonian of the form

$$\begin{aligned}
 \mathcal{H} = & \sum_{\text{Ln-ions}} D_{\text{Ln}}(S_Z^{\text{Ln}})^2 + \sum_{\text{Ni-ions}} D_{\text{Ni}}(S_Z^{\text{Ni}})^2 \\
 & + \sum_{\text{All-Clusters}} \left[ \sum_{\text{NiLn-Pairs}} J_{\text{NiLn}} S^{\text{Ni}} \cdot S^{\text{Ln}} + \sum_{\text{Ln-ions}} J_{\text{Ln}} S_i^{\text{Ln}} \cdot S_j^{\text{Ln}} \right] \\
 & + \sum_{\text{clusters}} J' S_i^{\text{cl}} \cdot S_j^{\text{cl}}
 \end{aligned} \quad (1)$$

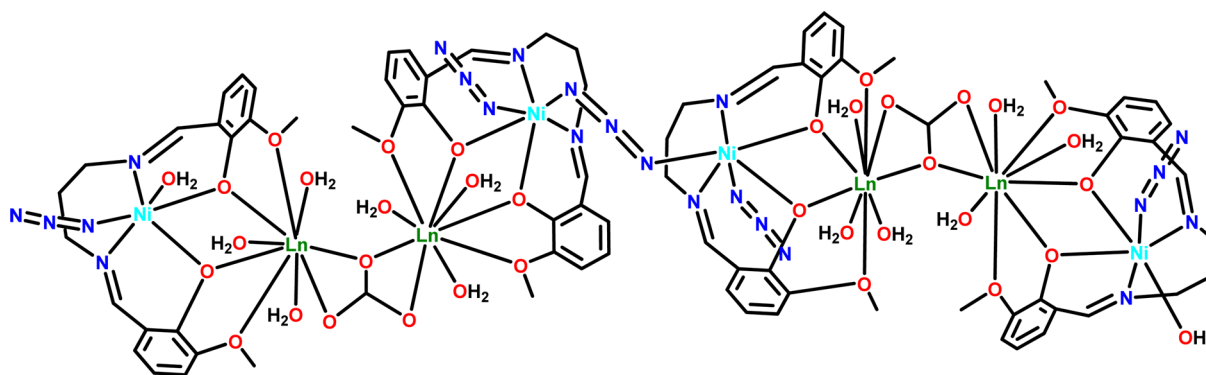


Figure 7. Molecular structure of a previously reported  $\text{Ni}_4\text{Ln}_4$  complex.<sup>25</sup>

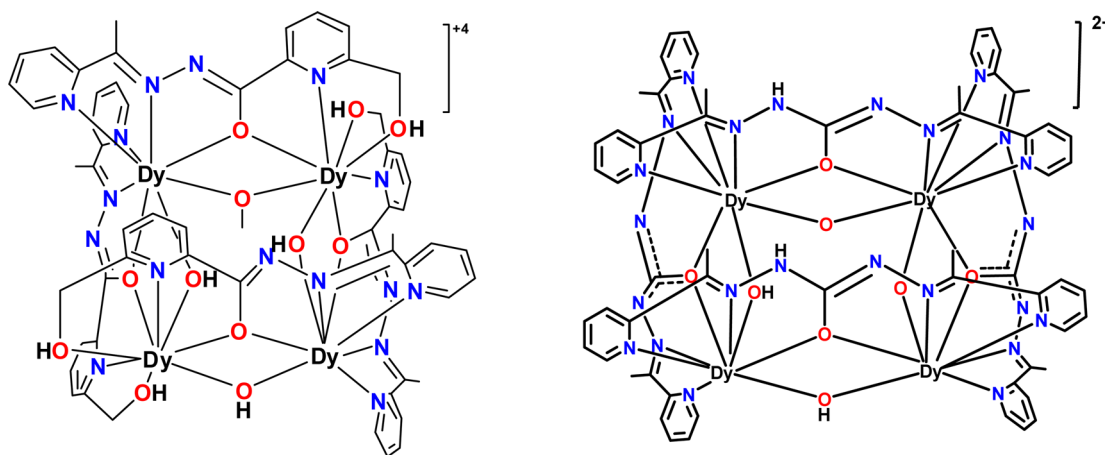


Figure 8. Line diagrams of reported  $\text{Dy}_4$  complexes having the  $[2 \times 2]$  square grid core.<sup>17,22c</sup>

Table 5. Comparison of Bond Lengths (Å) and Bond Angles (deg) in the Square-Grid Core Present in  $\text{Dy}_4$  Complexes

| complex  | Dy–O <sub>bridging</sub> | Dy–O <sub>alkoxy</sub> | Dy–OH–Dy | Dy–Dy | refs      |
|--|--------------------------|------------------------|----------|-------|-----------|
| $[\text{Dy}_4(\text{L})_4(\text{OH})_4]\cdot\text{Cl}_2$<br>$\text{H}_2\text{L} = 2\text{-}(1\text{-}(\text{pyridin-2-yl})\text{ethylidene})\text{hydrazinyl hydrazide}$   | 2.297                    |                        | 113.49   | 3.781 | 22c       |
| $[\text{Dy}_4(\text{HL})_4(\mu_2\text{-OH})_5(\mu_2\text{-OMe})]\cdot 4\text{NO}_3$<br>$\text{H}_2\text{L} = 6\text{-}(\text{hydroxymethyl})\text{-}N'\text{-}(1\text{-}(\text{pyridin-2-yl})\text{ethylidene})\text{picolinohydrazide}$ | 2.285                    | 2.402                  | 112.25   | 3.795 | 17        |
| $[\text{Dy}_4\text{Ni}_4(\text{H}_3\text{L})_4(\mu_3\text{-OH})_4(\mu_2\text{-OH})_4]$<br>$\text{H}_3\text{L} = N_1N_3\text{-bis}(6\text{-formyl-2-}(\text{hydroxymethyl})\text{-4-methylphenol})\text{ diethylenetriamine}$             | 2.406                    | 2.434                  | 102.04   | 3.741 | this work |

where the first two terms represent the  $\text{Ln}^{3+}$  and  $\text{Ni}^{2+}$  single-ion anisotropy, respectively. The term in square brackets represents the possible intracluster interactions, including Ni–Ln exchange ( $J_{\text{NiLn}}$ , an intradimer exchange described in the discussion below) and Ln–Ln exchange ( $J_{\text{LnLn}}$ , an interdimer exchange), and the last term represents exchange between clusters ( $J'$ ).  $S$  refers to the total (spin + orbital) angular momentum of a unit [an ion (Ni/Ln) or cluster (cl.)]

4f orbitals have a reduced spatial extent compared with 3d orbitals; hence, the consequently low-spin density between lanthanide ion centers implies  $J_{\text{NiLn}} \ll J_{\text{LnLn}}$ , while from distance arguments, it would be expected for the intercluster exchange to be the smallest exchange term. Therefore, each system likely consists of weakly interacting NiLn dimers. Furthermore, previous studies of  $\text{Ni}^{2+}$ – $\text{Ln}^{3+}$  compounds found the empirical rule that a ferromagnetic exchange existed when the  $\text{Ln}^{3+}$  ions contained greater than or half-filled 4f orbitals.<sup>26</sup> Thus, a ferromagnetic  $J_{\text{NiLn}}$  is expected for compounds 1–4. We note that while the intradimer exchange is depicted as Heisenberg in the above Hamiltonian, the  $\text{Ln}^{3+}$  ions  $\text{Dy}^{3+}$ ,  $\text{Tb}^{3+}$ , and  $\text{Ho}^{3+}$  are

known to exhibit highly anisotropic 4f electron clouds,<sup>27</sup> and so may lead to non-Heisenberg interactions. We present dc- and ac-magnetometry measurements performed on powdered samples to determine the relative importance of the single-ion anisotropy and interdimer interactions for each of the compounds in this heterometallic series.

**Compound 3,  $\text{Ni}_4\text{Gd}_4$ .** The lanthanide single-ion anisotropy term is expected to dominate in eq 1 for the  $\text{Dy}^{3+}$ ,  $\text{Tb}^{3+}$ , and  $\text{Ho}^{3+}$  congeners. However, since the electron distribution of spin-only  $\text{Gd}^{3+}$  ions exhibits a spherically symmetric electron cloud, the  $\text{Ni}_4\text{Gd}_4$  compound allows investigation of the single-ion anisotropy related solely to the  $\text{Ni}^{2+}$  ions.

The susceptibility of  $\text{Ni}_4\text{Gd}_4$  (Figure 10a) increases as temperature decreases in a Curie–Weiss manner. A deviation from this behavior is detected below 5 K, where  $\chi$  stabilizes at the lowest temperatures.

The product  $\chi_{\text{mol}}T$  of each material (Figure 10a, inset) shows a steady value at high temperatures indicating the compounds are in the paramagnetic phase where temperature fluctuations overcome all internal interactions. Here, each ion obeys  $\chi T =$



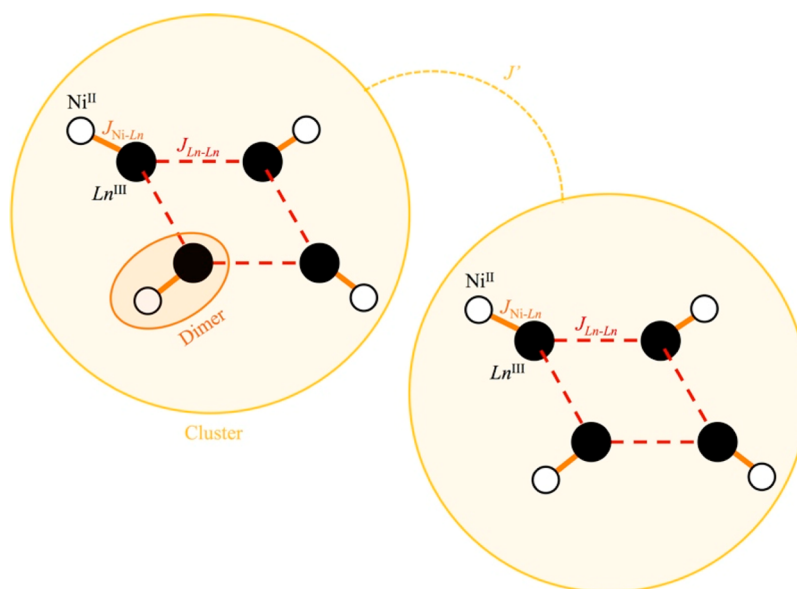


**Figure 9.** Schematic depiction of the inter- and intra-spin-exchange interactions described in the text for each  $\text{Ni}_4\text{Ln}_4$  unit (surrounding ligands are omitted for clarity).

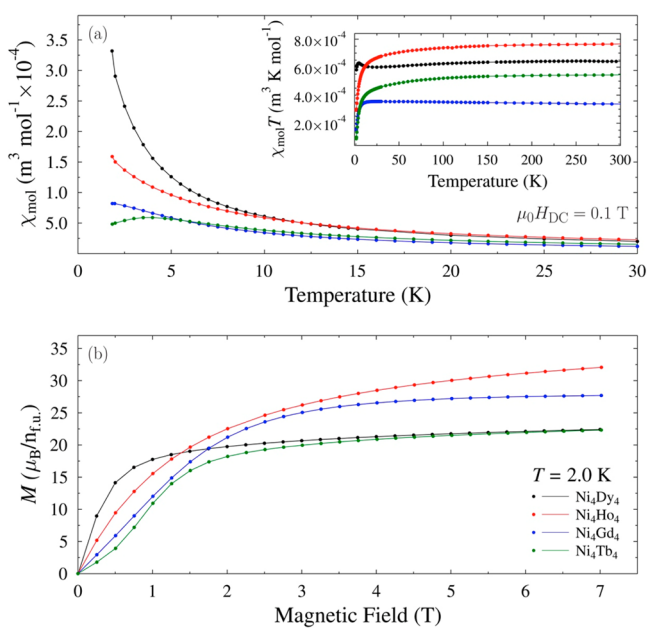


**Figure 10.** (a) Dc molar susceptibility of  $\text{Ni}_4\text{Dy}_4$  (black),  $\text{Ni}_4\text{Ho}_4$  (red),  $\text{Ni}_4\text{Gd}_4$  (blue), and  $\text{Ni}_4\text{Tb}_4$  (green) measured with  $\mu_0 H_{\text{DC}} = 0.1$  T. Inset: Product of the dc susceptibility,  $\chi_{\text{mol}} T$  vs  $T$ . (b) Isothermal magnetization vs applied dc-field for each compound at 2.0 K. Up sweeps only are shown for clarity. Units are  $\mu_{\text{B}}$  per formula unit ( $n_{\text{fu}}$ ).

$\mu_0 N_A \mu_{\text{eff}}^2 / (3k_{\text{B}})$  where  $\mu_{\text{eff}} = g_{\text{J}}(J(J+1))^{1/2} \mu_{\text{B}}$  and  $g_{\text{J}}$  is the Landé  $g$  factor.<sup>28</sup> The room-temperature value of  $\chi T$  was found to be within  $\sim 15\%$  of the expected value for each compound. Contributions to this result may come from (i) a strong single-ion anisotropy in the Dy, Ho, and Tb samples; (ii) diamagnetic contributions to the measurements of all samples from the sample holder, molecular ligands, and Vaseline; and (iii) small milligram losses of the sample incurred during the procedure to disperse the materials in the Vaseline. The  $\chi T$  data for  $\text{Ni}_4\text{Gd}_4$  features a small, negative gradient at high temperatures, which can be attributed to diamagnetic contributions from the

Vaseline, sample holder, and organic ligands. This diamagnetic component should be present for all compounds but is most obvious in the data for  $\text{Ni}_4\text{Gd}_4$ , which exhibits the smallest intrinsic room-temperature moment.

A rapid drop in  $\chi T$  for  $\text{Ni}_4\text{Gd}_4$  occurs in the region of  $T < 10$  K. Density functional theory calculations<sup>29</sup> predict that the Ni–Gd exchange interaction mediated through each of the three nonlinear Ni–O–Gd bonds should be ferromagnetic and have  $J_{\text{NiGd}} \approx 2.3$  K. The observed rapid decrease of  $\chi T$  on cooling can therefore be interpreted as due to a combination of the thermal depopulation of crystal-field split  $\text{Ni}^{2+}$  ion energy levels,<sup>30–32</sup> and the onset of Gd–Gd interactions. The onset of a low-temperature plateau in the susceptibility is indicative of single-ion anisotropy of the  $\text{Ni}^{2+}$  ions.<sup>33</sup> The lack of a Curie-like divergence of the susceptibility at low temperatures implies that the paramagnetic contribution to the measurement from the  $\text{Gd}^{3+}$  ions is reduced. Since spin-exchange interactions between lanthanide ions are expected to be small, we consider the effect of intracluster dipolar interactions. Treating  $\text{Gd}^{3+}$  and  $\text{Ni}^{2+}$  as classical moments, the energy of the cluster is defined as  $E = \mu_0 / 4\pi r^3 [\mu_1 \cdot \mu_2 - (\mu_1 \cdot \mathbf{r})(\mu_2 \cdot \mathbf{r}) / r^2]$  where  $\mu_{1,2}$  represents the magnetic moments of the considered ions and  $\mathbf{r}$  is the displacement vector between them.<sup>28</sup> The dipolar energy is minimized (by  $\sim 2.8$  K) on cooling by first allowing the  $\text{Gd}^{3+}$  moments to adopt a collinear antiparallel alignment, with moment directions perpendicular to the  $\text{Gd}^{3+}$  square plane. Since this occurs at a temperature scale exceeding the interdimer interaction, this implies that dipole–dipole interactions act to reduce the contribution of  $\text{Gd}^{3+}$  to the susceptibility at low temperatures and allow the data to stabilize.

For  $\text{Ni}^{2+}$  ions with an easy-plane single-ion anisotropy ( $D_{\text{Ni}}$ ), a minimum in  $d\chi/dT$  associated with the thermal depopulation of crystal-field split states is expected at  $T_{\text{min}} = 0.45 D_{\text{Ni}} / k_{\text{B}}$  (Figure S11). A minimum in  $d\chi/dT$  at 3.0(3) K for  $\text{Ni}_4\text{Gd}_4$  (Figure S11) lies above the Gd–Gd dipole–dipole energy, indicating it may be attributed to  $D_{\text{Ni}} = 6.7(7)$  K.

The magnetization of  $\text{Ni}_4\text{Gd}_4$  [Figure 10b] follows a steady, near linear increase toward a value of  $M = 25 \mu_{\text{B}} / n_{\text{fu}}$  at  $\mu_0 H_{\text{DC}} =$

7 T, which is lower than the saturation magnetization of  $36.0 \mu_{\text{B}}/n_{\text{f.u.}}$  for paramagnetic  $\text{Ni}^{2+}$  and  $\text{Gd}^{3+}$ . This is consistent with the development of anisotropic  $\text{Ni}^{2+}$  ions at low temperatures.

Ac susceptibility measurements of  $\text{Ni}_4\text{Gd}_4$  with  $\mu_0 H_{\text{DC}} = 0$  T [Figure 11a,c] indicate that  $\chi'$  increases on cooling with no

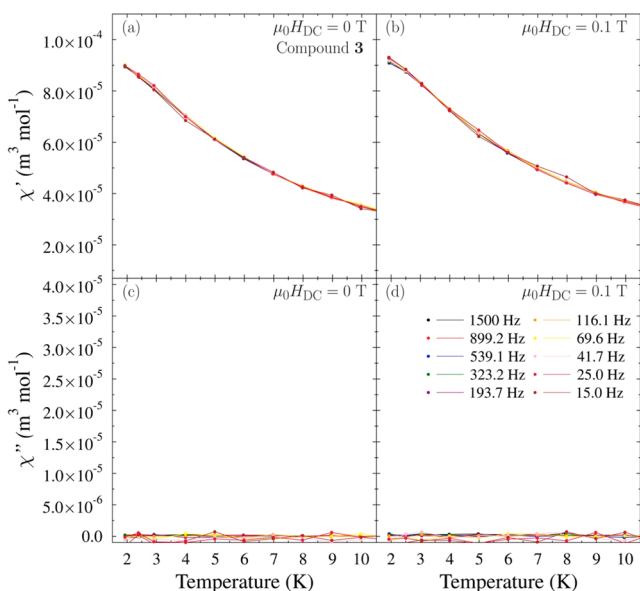


**Figure 11.** Ac susceptibility of  $\text{Ni}_4\text{Gd}_4$  reported as the in-phase and out-of-phase susceptibility,  $\chi'$  and  $\chi''$ , in a dc magnetic field of  $\mu_0 H_{\text{DC}} = 0$  T in a and c and a magnetic field of  $\mu_0 H_{\text{DC}} = 0.1$  T in b and d.

evidence of frequency separation for ac-field frequencies  $\leq 1500$  Hz. The lack of slow relaxation in the magnetization is further supported by measurements obtained when a dc field of  $\mu_0 H_{\text{DC}} = 0.1$  T is applied. We note a very weak frequency dependence below 2.0 K, which may be attributed to the induced slow-relaxation expected when the degeneracy of the spin-states of the paramagnetic  $\text{Gd}^{3+}$  ions is lifted by the 0.1 T magnetic field.<sup>34,35</sup>

In combination with observations from dc measurements, this indicates that while  $\text{Ni}_4\text{Gd}_4$  does contain a nonzero anisotropy related to  $\text{Ni}^{2+}$ , it is easy plane (i.e.,  $D_{\text{Ni}} > 0$ ) rather than the Ising-like anisotropy required for slow relaxation of magnetization.<sup>36–38</sup>

**Compound 4,  $\text{Ni}_4\text{Ho}_4$ .** The high-temperature dc susceptibility of  $\text{Ni}_4\text{Ho}_4$  [Figure 10a] increases on cooling in a Curie–Weiss manner. This behavior leads to the steady high temperature plateau observed in  $\chi T$ , which agrees well with the value expected for independent paramagnetic ions. The decrease observed in  $\chi T$  on cooling occurs at a much higher temperature than that for  $\text{Ni}_4\text{Gd}_4$ , indicating a different physical origin for this behavior.  $\text{Ho}^{3+}$  has a highly anisotropic electron distribution,<sup>27</sup> such that it would be expected that  $|D_{\text{Ho}}| \gg |D_{\text{Ni}}|$ . Thus, this  $\chi T$  decrease can be attributed to the large single-ion anisotropy of the  $\text{Ho}^{3+}$  ions. The fact that  $\chi$  continues to increase down to low temperatures implies that there are no significant antiferromagnetic interactions between  $\text{Ho}^{3+}$  ions for the temperature range studied. Furthermore, any Ni–Ho exchange is expected to be ferromagnetic in nature,<sup>26</sup> so the lack of an increase in  $\chi T$  or hysteresis in the magnetization (Figure 10b) indicates that the magnetic properties of this material are dominated by the single-ion properties of individual  $\text{Ni}^{2+}$  and  $\text{Ho}^{3+}$  ions. The slowly rising

magnetization reaches a value of  $32 \mu_{\text{B}}/n_{\text{f.u.}}$  at 7 T, which is much less than the predicted saturation magnetization of individual ions of  $50.7 \mu_{\text{B}}/n_{\text{f.u.}}$  and therefore supports the conclusion of a large  $D_{\text{Ho}}$  in this material.

A complete lack of frequency or dc magnetic field dependence in  $\chi'$  and the observation of a near-zero  $\chi''$  response (Figure 12) indicate that  $\text{Ni}_4\text{Ho}_4$  shows no slow SMM relaxation. This is consistent with the presence of a large easy-plane single-ion anisotropy of the  $\text{Ho}^{3+}$  ions.

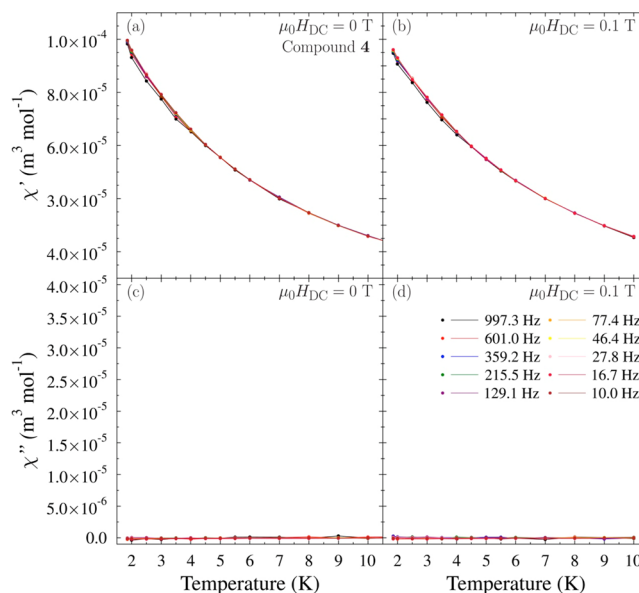


**Figure 12.** Ac susceptibility of  $\text{Ni}_4\text{Ho}_4$  reported as the in-phase and out-of-phase susceptibility,  $\chi'$  and  $\chi''$ , in a dc magnetic field of  $\mu_0 H_{\text{DC}} = 0$  T in a and c and a magnetic field of  $\mu_0 H_{\text{DC}} = 0.1$  T in b and d.

**Compound 1,  $\text{Ni}_4\text{Dy}_4$ .** The  $\chi T$  data for  $\text{Ni}_4\text{Dy}_4$  (Figure 10a) initially decreases from the room temperature value on cooling and by analogy to the  $\text{Ho}^{3+}$  congener; this is associated with the thermal depopulation of the lanthanide ion's spin states. On further reduction of the temperature, a peak centered at approximately 4.8 K is observed. A similar feature has previously been observed in  $\text{Dy}^{3+}$  and  $\text{Tb}^{3+}$  cluster compounds displaying SMM behavior and attributed to intracenter interactions.<sup>31,39</sup> Furthermore, in Ni–Ln coupled systems, such a peak has been identified as due to ferromagnetic exchange between  $\text{Ni}^{2+}$  and  $\text{Ln}^{3+}$ .<sup>26</sup>

The magnetization of  $\text{Ni}_4\text{Dy}_4$  (Figure 10b) shows the most rapid initial increase of any member of this series of magnets, with a transition to a slower increase above 1 T. The moment of  $22.5 \mu_{\text{B}}/n_{\text{f.u.}}$  at 7 T is far less than the saturation value for individual ions of  $48.0 \mu_{\text{B}}/n_{\text{f.u.}}$ , which is indicative of the single-ion anisotropy of the  $\text{Ni}^{2+}$  and  $\text{Dy}^{3+}$  as well as the presence of Dy–Ni interactions.

The ac susceptibility performed at both  $\mu_0 H_{\text{DC}} = 0$  and 0.14 T is shown in Figure 13. For  $\mu_0 H_{\text{DC}} = 0$  T, a clear frequency dependence is evident, whereby the in-phase susceptibility shows a weak separation of frequencies at low-temperatures, accompanied by a nonzero, frequency-dependent out-of-phase susceptibility signal below 8 K caused by the presence of slow magnetization dynamics. This bears a strong resemblance to previously reported SMMs in which zero-field slow relaxation was suppressed by quantum tunneling of magnetization (QTM).<sup>30,32,40</sup>

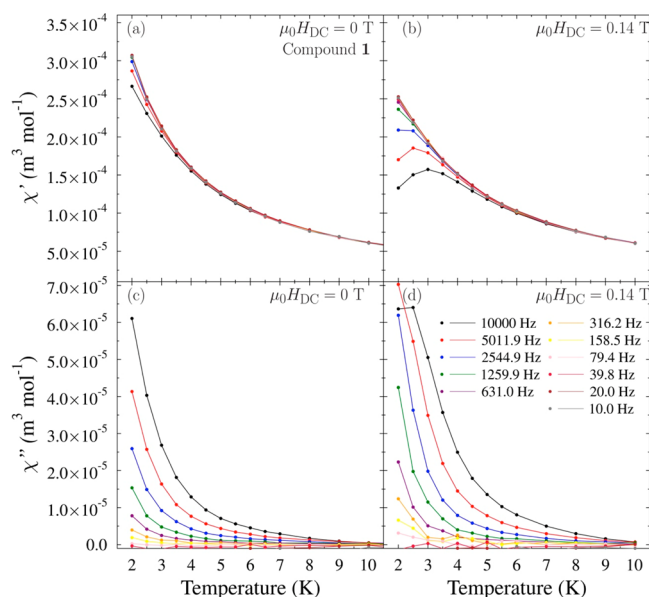


**Figure 13.** Ac susceptibility of  $\text{Ni}_4\text{Dy}_4$  reported as the in-phase and out-of-phase susceptibility,  $\chi'$  and  $\chi''$ , in a dc magnetic field of  $\mu_0 H_{\text{DC}} = 0$  T in a and c and a magnetic field of  $\mu_0 H_{\text{DC}} = 0.14$  T in b and d.

On applying the derived optimum field of  $\mu_0 H_{\text{DC}} = 0.14$  T (Figure 13c,d and Figure S13), the frequency dependence of  $\chi'$  can be seen to become enhanced and be driven to higher temperatures with peaks occurring at the highest frequencies. This may be explained as due to the single-ion anisotropy of  $\text{Dy}^{3+}$ .  $\text{Dy}^{3+}$  is a Kramers ion ( $S = 15/2$ ), which contains a ground state doublet in zero applied dc magnetic field.<sup>5,30</sup> Thus, while phonon assisted relaxation of the magnetization is possible in an applied ac-field, this relaxation mechanism can be suppressed in favor of the faster QTM within the bistable ground state.<sup>30</sup> The application of a dc magnetic field, however, lifts the ground-state degeneracy and suppresses QTM, allowing phonon assisted relaxation to become the dominant relaxation mechanism.<sup>37</sup> In this situation, peaks occur in  $\chi''(T)$  corresponding to the temperature when the ac-field angular frequency ( $\omega$ ) and relaxation time ( $\tau$ ) satisfy  $\omega\tau = 1$ .<sup>34</sup>

A Cole–Cole plot is presented in Figure 14. The data follow single, isothermal arcs that become more complete as temperature decreases, suggesting the presence of single relaxation pathways.<sup>34,41</sup> The data at 2 K are compared to the generalized Debye model to determine the isothermal and adiabatic susceptibility,  $\chi_T$  and  $\chi_S$  and spread of relaxation times,  $\alpha$ .<sup>32</sup> A fit to this model (S3) yields the parameters  $\chi_T = 2.491(7) \times 10^{-4} \text{ m}^3 \text{ mol}^{-1}$ ,  $\chi_S = 9.6(9) \times 10^{-5} \text{ m}^3 \text{ mol}^{-1}$ , and  $\alpha = 0.03(4)$ . The low value of  $\alpha$  represents a small distribution of relaxation times, which is further indicative of a single relaxation mechanism. While only one peak can be observed in  $\chi''(T)$  (Figure 13d), the form of the ac susceptibility data offers strong evidence that  $\text{Ni}_4\text{Dy}_4$  is a field-induced SMM. However, higher frequencies or lower temperatures would be required to fully quantify this slow relaxation and derive a value for the energy barrier to slow relaxation,  $U_{\text{eff}}$  via Arrhenius analysis.

The observation of weak SMM behavior in  $\text{Ni}_4\text{Dy}_4$  results from the easy-axis anisotropy developed by the Kramers  $\text{Dy}^{3+}$  ions in the distorted square antiprism coordination environment (Figure 6b). This Ising character is a consequence of a preferred orientation of the oblate<sup>27</sup> 4f electron cloud due to an electrostatic interaction with the surrounding negative

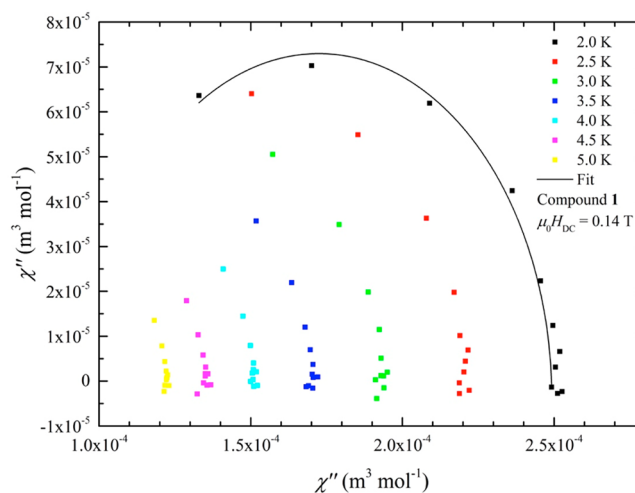


**Figure 14.** Cole–Cole plot of  $\text{Ni}_4\text{Dy}_4$  as measured in a magnetic field of  $\mu_0 H_{\text{DC}} = 0.14$  T including a fit to the generalized Debye model.

ligands. Given that the coordination environment of the  $\text{Ho}^{3+}$  ions in  $\text{Ni}_4\text{Ho}_4$  is similar (Figure S6), the smaller spatial extent of the 4f electron cloud in each lanthanide center relative to the  $\text{Dy}^{3+}$  congener is likely to weaken the effects of the crystal field at the  $\text{Ho}^{3+}$  magnetic centers. The lack of SMM characteristics in the dynamic susceptibility study of this non-Kramers system is also further indicative of an easy-plane ground state for the  $\text{Ho}^{3+}$  ions.

**Compound 2,  $\text{Ni}_4\text{Tb}_4$ .** The  $\chi T$  data for  $\text{Ni}_4\text{Tb}_4$  (inset to Figure 10a) are similar to that of  $\text{Ni}_4\text{Ho}_4$ . A decrease is observed from a steady value at temperatures below  $\sim 100$  K that may be attributed to the thermal depopulation of  $\text{Tb}^{3+}$  spin states. For the non-Kramers  $\text{Tb}^{3+}$  ions, a bistable ground state may only be realized if the crystal field at the lanthanide centers is strictly axial.<sup>27</sup> Since the point group at the  $\text{Tb}^{3+}$  lattice sites is determined to be 1, each ion can be assigned a ground-state singlet such that the single-ion anisotropy is easy plane in nature. This argument can be extended by analogy to  $\text{Ni}_4\text{Ho}_4$  as further evidence of easy-plane  $\text{Ho}^{3+}$  anisotropy as  $\text{Ho}^{3+}$  is also a non-Kramers ion with the same point group symmetry on the  $\text{Ho}^{3+}$  lattice site.

The decrease in  $\chi T$  becomes more pronounced as the temperature is reduced further from 10 to 5 K. This feature is also observed for both the  $\text{Ho}^{3+}$  and  $\text{Gd}^{3+}$  members of this heterometallic series, which implies that this shared behavior may be associated with the thermal depopulation of  $\text{Ni}^{2+}$  crystal-field split energy levels.

The lack of a peak in  $\chi T$  in  $\text{Ni}_4\text{Tb}_4$  below 5 K is in contrast to the behavior of the  $\text{Dy}^{3+}$  congener, which is indicative of the absence of ferromagnetic Ni–Tb interactions in the former material.<sup>26</sup> Furthermore, the rounded maximum at 3.9(3) K in the dc susceptibility of  $\text{Ni}_4\text{Tb}_4$  (Figure 10a) contrasts with the leveling out observed in  $\text{Ni}_4\text{Gd}_4$  that was attributed to the single-ion anisotropy of the  $\text{Ni}^{2+}$  ions and a cancellation of the lanthanide moments' contribution to the measurement. We suggest that these two observations for the  $\text{Ni}_4\text{Tb}_4$  material, together with the ac susceptibility data discussed below, are consistent with a model for which the Ni–Tb exchange interactions are antiferromagnetic. The maximum in the susceptibility is then achieved from an overall cancellation of each dimer's moment due to interdimer interactions that arise from the dipolar coupling expected to be significant in these

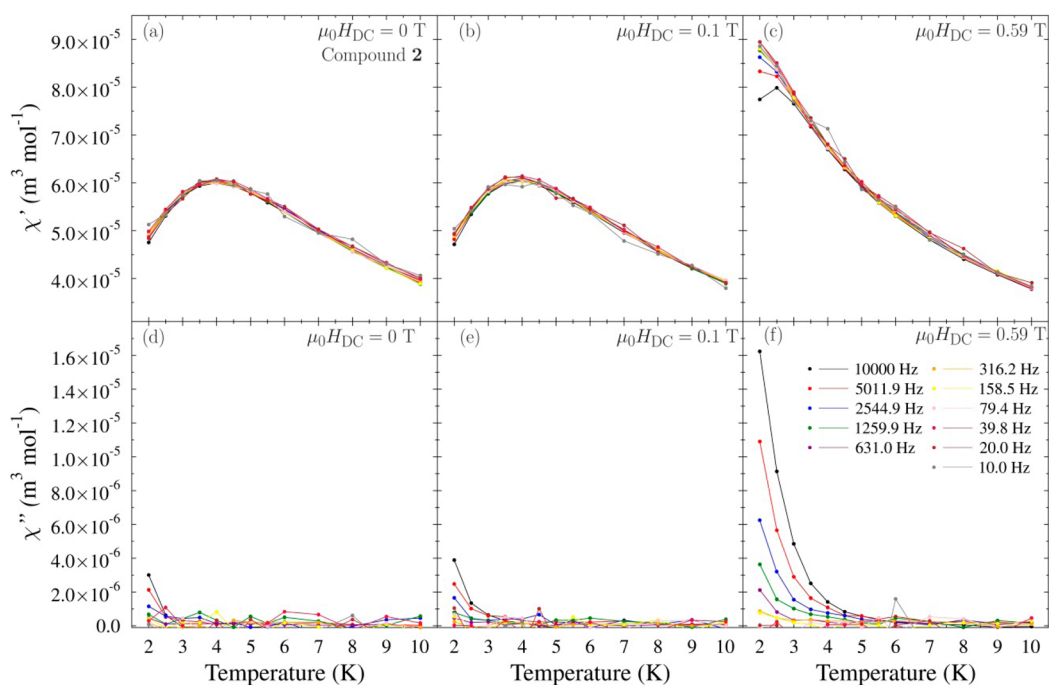


**Figure 15.** Ac susceptibility of  $\text{Ni}_4\text{Tb}_4$  measured on cooling in (a, d)  $\mu_0 H_{\text{DC}} = 0$  T, (b, e)  $\mu_0 H_{\text{DC}} = 0.1$  T, and (c, f)  $\mu_0 H_{\text{DC}} = 0.59$  T. An ac magnetic field amplitude of  $\mu_0 H_{\text{AC}} = 0.1$  mT is used for frequencies above 1500 Hz; otherwise,  $\mu_0 H_{\text{AC}} = 0.4$  T.

materials at low temperatures.  $\text{Ni}_4\text{Tb}_4$  therefore may provide a counterexample to the aforementioned empirical rule that predicts a ferromagnetic exchange between  $\text{Ni}^{2+}$  and  $\text{Ln}^{3+}$  centers.<sup>26</sup> This likely results from the precise form of the Ni–Ln exchange pathways afforded by the ligand architecture and spin density in these systems. We also note that the  $\text{Ho}^{3+}$  and  $\text{Gd}^{3+}$  members of this heterometallic series offer no evidence for ferromagnetic Ni–Ln exchange.

The ac susceptibility of  $\text{Ni}_4\text{Tb}_4$  in both  $\mu_0 H_{\text{DC}} = 0$  T (Figure 15a,d) and  $\mu_0 H_{\text{DC}} = 0.1$  T (Figure 15b,e) lacks a strong out-of-phase component to the measurement. The absence of field induced slow-relaxation is consistent with the easy-plane anisotropy assigned to the lanthanide moments. A field dependent study of the dynamic susceptibility (Supporting Information) revealed that an out-of-phase component may be induced in larger applied fields, with the slow-relaxation for  $\mu_0 H_{\text{DC}} = 0.59$  T (Figure 15c,f) exhibiting both a frequency-dependent maximum in  $\chi'$  and an order of magnitude increase in  $\chi''$  relative to the low dc-field measurements. Furthermore, the position of the maximum in  $\chi'$  decreases in temperature when the dc field is increased, which is consistent with the attribution of this feature to the formation of antiferromagnetic dimers in the preceding discussion.

The qualitative similarity of the ac susceptibility for  $\mu_0 H_{\text{DC}} = 0.59$  T to the slow relaxation observed in the  $\text{Dy}^{3+}$  material (Figure 13) is indicative of slow relaxation via a single pathway in  $\text{Ni}_4\text{Tb}_4$ . This conclusion is further supported by a comparison of Cole–Cole plots of the  $\text{Tb}^{3+}$  material's ac susceptibility data collected in nonzero dc fields (Figure 16). For  $\mu_0 H_{\text{DC}} = 0.59$  T, isotherms in the  $\chi' - \chi''$  plane appear to form extended arcs that become more extended on cooling, as predicted by the modified Debye model,<sup>34</sup> whereas the behavior for  $\mu_0 H_{\text{DC}} = 0.1$  T shows a temperature dependence that is incompatible with traditional SMM behavior.

The onset of the slow relaxation in the ac susceptibility at  $\mu_0 H_{\text{DC}} = 0.59$  T is concurrent with a sudden rapid rise in the

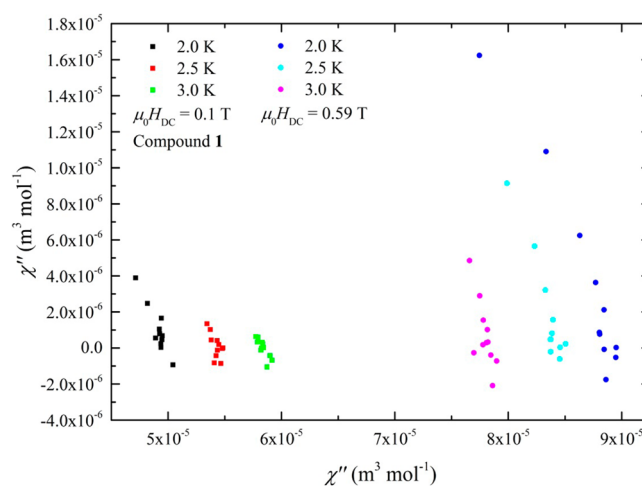


**Figure 16.** Cole–Cole plot for  $\text{Ni}_4\text{Tb}_4$  in  $\mu_0 H_{\text{DC}} = 0.1$  and  $0.59$  T for constant temperatures in the range  $2 \leq T \leq 3$  K. The data collected in  $0.59$  T resemble the development of large semicircular arcs on cooling expected from the modified Debye model for single pathway slow relaxation (Figure 14).

magnetization of the powdered sample in a dc field (Figure 10b). This implies that, at this point, a larger fraction of the sample moments may align to the applied field while the material also adopts a magnetic easy axis to permit the slow-relaxing behavior. To explain both phenomena, we consider a model Hamiltonian for each Ni–Tb dimer, appropriate at low temperatures and small applied fields, of the form:

$$\mathcal{H} = J_{\text{NiTb}} S^{\text{Ni}} \cdot S^{\text{Tb}} + D_{\text{Dimer}} S_Z^2 + g \mu_B S \cdot H \quad (2)$$

where  $S^{\text{Ni}} = 1$  is the  $\text{Ni}^{2+}$  spin,  $S^{\text{Tb}} = 6$  is the  $\text{Tb}^{3+}$  total angular momentum, and the dimerized unit has total spin  $S$  and  $g$  factor,  $g$ . The antiferromagnetic Heisenberg intradimer spin-exchange term,  $J_{\text{NiTb}}$ , favors the low-spin ( $S = 5$ ) state, while the

anisotropy of the dimers results from the coupling of two anisotropic moments and is parametrized with  $D_{\text{Dimer}}$ . Here,  $D_{\text{Dimer}} > 0$  is dominated by the contribution from the easy-plane  $\text{Tb}^{3+}$  moments, such that within the  $S = 5$  multiplet the ground state is the  $M_S = 0$  singlet while the  $M_S = \pm 1$  doublet forms the first excited state.

This model achieves the ground-state singlet necessary to explain the form of the dc and ac susceptibility in dc fields  $\mu_0 H_{\text{DC}} \leq 0.1$  T. For dc fields applied perpendicular to the easy plane, the field induced Zeeman splitting of the  $M_S = \pm 1$  doublet may close the zero-field spin-gap, resulting in a level crossing to a magnetic ground state. At this crossing, a sharp step-like increase in the magnetization is expected. For a polycrystalline measurement of the magnetization, in which the field is applied at all angles to the easy plane for different portions of the sample, this step-like feature will be broadened by powder averaging. We therefore attribute the rounded increase in the magnetization for  $\text{Ni}_4\text{Tb}_4$  at  $\mu_0 H_{\text{DC}} \approx 0.6$  T to the closing of the spin-gap in the AFM Ni–Tb dimer states by the applied field. Furthermore, the development of a magnetic ground state at this point with an axial component of the magnetic moment permits the development of the slow relaxation that is observed at the same field. This slow relaxation of magnetization results from the small energy barrier for the reorientation of the dimer moments in an oscillating field when two magnetic states of differing  $M_S$  are close to degenerate as the spin gap is closed. If the applied field is increased above 0.6 T, the out-of-phase susceptibility falls once again (Supporting Information) since the bistability of the system is detuned and the system reverts to a singlet ground state. This field dependence of the ac susceptibility is an interesting contrast to field-induced SMMs in which SMM behavior is suppressed at zero fields by QTM.<sup>30,32,40</sup>

## SUMMARY

Utilizing a new compartmental Schiff base ligand containing a crucial  $-\text{CH}_2\text{OH}$  motif, we were able to assemble octanuclear complexes,  $\{\text{Ni}_4\text{Ln}_4\}$ , possessing a central  $\text{Ln}_4$  grid topology supporting four peripheral  $\text{Ni}^{\text{II}}$  centers. To the best of our knowledge, such a structural topology is unique among the 3d/4f family.

We have measured the dc and ac susceptibilities of the  $\text{Ni}_4\text{Ln}_4$  family (where  $\text{Ln} = \text{Dy}^{3+}$ ,  $\text{Gd}^{3+}$ ,  $\text{Ho}^{3+}$ , and  $\text{Tb}^{3+}$ , compounds 1–4, respectively).  $\text{Ni}_4\text{Gd}_4$  is found to contain  $\text{Ni}^{2+}$  ions with easy-plane anisotropy of an estimated value of  $D_{\text{Ni}} = 6.7(7)$  K. A nonzero  $D_{\text{Ni}}$  is evidenced by a plateau of dc magnetic susceptibility, which also suggests a reduced contribution to the measurement from the  $\text{Gd}^{3+}$  ions that we attribute to dipolar interactions between the lanthanide ions.

$\text{Ni}_4\text{Ho}_4$  is found to exhibit a much larger single-ion anisotropy associated with the anisotropic 4f electron cloud of  $\text{Ho}^{3+}$ . This manifests itself as a decrease of the product  $\chi T$  on cooling due to the thermal depopulation of  $\text{Ho}^{3+}$  energy levels. Dc susceptibility measurements exhibit no evidence of ferromagnetic Ni–Ho interactions for  $T > 2$  K, and the lack of slow relaxation in ac susceptibility measurements is consistent with a singlet ground state for the non-Kramers  $\text{Ho}^{3+}$  ions.

$\text{Ni}_4\text{Dy}_4$  is found to contain large single-ion anisotropy of the  $\text{Dy}^{3+}$  moments. Furthermore, ferromagnetic Ni–Dy interactions are evident from a small peak in  $\chi T$  below 5 K. As  $\text{Dy}^{3+}$  is a Kramers ion, an easy-axis single-ion anisotropy is guaranteed and is confirmed by the presence of slow relaxation in ac

susceptibility measurements. The SMM behavior is enhanced by the application of a dc magnetic field that lifts the degeneracy of the bistable ground state and alleviates the effects of QTM that suppress the slow relaxation in zero field.

For  $\text{Ni}_4\text{Tb}_4$ , a decrease in the product  $\chi T$  below  $T \approx 100$  K suggests large single-ion anisotropy associated with  $\text{Tb}^{3+}$  ions, and the low temperature dc susceptibility is consistent with the formation of antiferromagnetic Ni–Tb dimers.  $\text{Tb}^{3+}$  is a non-Kramers ion and occupies lattice sites that provide a crystal field that lacks axial symmetry; hence the magnetic anisotropy at low temperatures is expected to be easy plane. This is supported by ac measurements, which, at low dc fields, show no strong slow relaxation of magnetization. The presence of slow relaxation in dc fields of 0.59 T was attributed to a level crossing to a magnetic ground state at this field that also induces a sharp increase in the dc magnetization at this point. As such, we suggest that the slow relaxation in  $\text{Ni}_4\text{Tb}_4$  is suppressed in low fields not by QTM, but rather the easy-plane anisotropy of Ni–Tb dimers.

## ASSOCIATED CONTENT

### Supporting Information

The Supporting Information is available free of charge on the ACS Publications website at DOI: 10.1021/acs.inorgchem.6b01019.

ESI-MS spectra, molecular structure, and a list of bond lengths and angles of the complexes 2, 3, and 4. Crystal packing diagram of 1 and hydrogen bonding structure of 1. Simulated dc magnetic susceptibility curves of normalized  $\chi$ ,  $\chi T$ , and  $d\chi/dT$  against normalized temperature for  $\text{Ni}^{2+}$  ions of easy-plane single-ion anisotropy. Dc magnetic susceptibility of 3 differentiated with respect to  $T$ ,  $d\chi/dT$ , magnetic field study of 1 at 2 K via ac susceptibility measurements, frequency dependence ac susceptibility plot of 1, and magnetic field study of 2 at 2 K (PDF)

Crystallographic data for the structures in this paper (CIF)

## AUTHOR INFORMATION

### Corresponding Authors

\*E-mail: p.goddard@warwick.ac.uk.

\*E-mail: vc@iitk.ac.in and vc@niser.ac.in.

### Notes

The authors declare no competing financial interest.

## ACKNOWLEDGMENTS

We thank the Department of Science and Technology (DST), India, for financial support, including support for a Single Crystal CCD X-ray Diffractometer facility at IIT-Kanpur. V.C. is grateful to the DST for a J. C. Bose fellowship. S.B., J.G., and S.D. thank the Council of Scientific and Industrial Research, India for a Senior Research Fellowship. We would like to thank Gavin Stenning for help on the Quantum Design PPMS instrument in the Materials Characterisation Laboratory at the ISIS Neutron and Muon Source. C.V.T. thanks Dharmalingham Prabhakaran and Stephen Blundell for experimental assistance and useful discussions. J.B., P.G., and C.V.T. thank the EPSRC for support. Data presented in this paper resulting from the UK effort will be made available at <http://wrap.warwick.ac.uk/80503/>.

## REFERENCES

- (1) (a) Sessoli, R.; Gatteschi, D.; Caneschi, A.; Novak, M. A. *Nature* **1993**, *365*, 141–143. (b) Sessoli, R.; Tsai, H. L.; Schake, A. R.; Wang, S.; Vincent, J. B.; Folting, K.; Gatteschi, D.; Christou, G.; Hendrickson, D. N. *J. Am. Chem. Soc.* **1993**, *115*, 1804–1816.
- (2) (a) Leuenberger, M. N.; Loss, D. *Nature* **2001**, *410*, 789–793. (b) Hill, S.; Edwards, R. S.; Aliaga-Alcalde, N.; Christou, G. *Science* **2003**, *302*, 1015–1018.
- (3) (a) Mannini, M.; Pineider, F.; Danieli, C.; Totti, F.; Sorace, L.; Sainctavit, P.; Arrio, M. A.; Otero, E.; Joly, L.; Cezar, J. C.; Cornia, A.; Sessoli, R. *Nature* **2010**, *468*, 417–421. (b) Urdampilleta, M.; Nguyen, N. V.; Cleuziou, J. P.; Klyatskaya, S.; Ruben, M.; Wernsdorfer, W. *Int. J. Mol. Sci.* **2011**, *12*, 6656. (c) Bürgler, D. E.; Heß, V.; Esat, T.; Fahrendorf, S.; Matthes, F.; Schneider, C. M.; Besson, C.; Monakhov, K.; Yu, Kögerler, P.; Ghisolfi, A.; Braunstein, P.; Atodiresi, N.; Caciuc, V.; Blügel, S. *e-J. Surf. Sci. Nanotechnol.* **2016**, *14*, 17–22.
- (4) (a) Coronado, E.; Day, P. *Chem. Rev.* **2004**, *104*, 5419–5448. (b) Bogani, L.; Wernsdorfer, W. *Nat. Mater.* **2008**, *7*, 179–186. (c) Woodruff, D. N.; Winpenny, R. E. P.; Layfield, R. A. *Chem. Rev.* **2013**, *113*, 5110–5148.
- (5) (a) Chandrasekhar, V.; Dey, A.; Mota, A. J.; Colacio, E. *Inorg. Chem.* **2013**, *52*, 4554–4561. (b) Glaser, T. *Chem. Commun.* **2011**, *47*, 116–130. (c) Boukhalov, D. W.; Dobrovitski, V. V.; Kögerler, P.; Al-Saqer, M.; Katsnelson, M. I.; Lichtenstein, A. I.; Harmon, B. N. *Inorg. Chem.* **2010**, *49*, 10902–10906. (d) Inglis, R.; Jones, L. F.; Karotsis, G.; Collins, A.; Parsons, S.; Perlepes, S. P.; Wernsdorfer, W.; Brechin, K. E. *Chem. Commun.* **2008**, 5924–5926. (e) Terazzi, E.; Rogez, G.; Gallani, J. L.; Donnio, B. *J. Am. Chem. Soc.* **2013**, *135*, 2708–2722.
- (6) (a) Das, S.; Hossain, S.; Dey, A.; Biswas, S.; Sutter, J.-P.; Chandrasekhar, V. *Inorg. Chem.* **2014**, *53*, 5020–5028. (b) Baldoví, J. J.; Cardona-Serra, S.; Clemente-Juan, J. M.; Coronado, E.; Gaita-Ariño, A.; Palií, A. *Inorg. Chem.* **2012**, *51*, 12565–12574. (c) Das, S.; Dey, A.; Biswas, S.; Colacio, E.; Chandrasekhar, V. *Inorg. Chem.* **2014**, *53*, 3417–3426. (d) Biswas, S.; Jena, H. S.; Adhikary, A.; Konar, S. *Inorg. Chem.* **2014**, *53*, 3926–3928. (e) Chandrasekhar, V.; Bag, P.; Colacio, E. *Inorg. Chem.* **2013**, *52*, 4562–4570. (f) Goswami, S.; Adhikary, A.; Jena, H. S.; Konar, S. *Dalton Trans.* **2013**, *42*, 9813–9817. (g) Goura, J.; Walsh, J. P. S.; Tuna, F.; Chandrasekhar, V. *Inorg. Chem.* **2014**, *53*, 3385–3391. (h) Joarder, B.; Chaudhari, A. K.; Rogez, G.; Ghosh, S. K. *Dalton Trans.* **2012**, *41*, 7695–7699. (i) Biswas, S.; Mondal, A.; Konar, S. *Inorg. Chem.* **2016**, *55*, 2085–2090. (j) Mondal, A.; Parmar, V. S.; Biswas, S.; Konar, S. *Dalton Trans.* **2016**, *45*, 4548–4557.
- (7) (a) Andruh, M.; Costes, J.-P.; Diaz, C.; Gao, S. *Inorg. Chem.* **2009**, *48*, 3342–3359. (b) Winpenny, R. E. P. *Chem. Soc. Rev.* **1998**, *27*, 447–452. (c) Schray, D.; Abbas, G.; Lan, Y.; Mereacre, V.; Sundt, A.; Dreiser, J.; Waldmann, O.; Kostakis, G. E.; Anson, C. E.; Powell, A. K. *Angew. Chem., Int. Ed.* **2010**, *49*, 5185–5188. (d) Chandrasekhar, V.; Pandian, B. M.; Vittal, J. J.; Clérac, R. *Inorg. Chem.* **2009**, *48*, 1148–1157. (e) Mondal, K. C.; Sundt, A.; Lan, Y.; Kostakis, G. E.; Waldmann, O.; Ungur, L.; Chibotaru, L. F.; Anson, C. E.; Powell, A. K. *Angew. Chem., Int. Ed.* **2012**, *51*, 7550–7554. (f) Meseguer, C.; Titos-Padilla, S.; Hänninen, M. M.; Navarrete, R.; Mota, A. J.; Evangelisti, M.; Ruiz, J.; Colacio, E. *Inorg. Chem.* **2014**, *53*, 12092–12099. (g) Goura, J.; Guillaume, R.; Rivière, E.; Chandrasekhar, V. *Inorg. Chem.* **2014**, *53*, 7815–7823. (h) Das, S.; Bejoramohandas, K. S.; Dey, A.; Biswas, S.; Reddy, M. L. P.; Morales, R.; Ruiz, E.; Titos-Padilla, S. T.; Colacio, E.; Chandrasekhar, V. *Chem. - Eur. J.* **2015**, *21*, 6449–6464. (i) Terazzi, E.; Rogez, G.; Gallani, J.-L.; Donnio, B. *J. Am. Chem. Soc.* **2013**, *135*, 2708–2722.
- (8) (a) Rinehart, J. D.; Fang, M.; Evans, W. J.; Long, J. R. *J. Am. Chem. Soc.* **2011**, *133*, 14236–14239.
- (9) (a) Hendrickson, D. N.; Christou, G.; Ishimoto, H.; Yoo, J.; Brechin, E. K.; Yamaguchi, A.; Rumberger, E. M.; Aubin, S. M. J.; Sun, Z.; Aromi, G. *Polyhedron* **2001**, *20*, 1479–1488.
- (10) (a) Langley, S. K.; Forsyth, C. M.; Moubaraki, B.; Murray, K. S. *Dalton Trans.* **2015**, *44*, 912–915. (b) Langley, S. K.; Wielechowski, P. D.; Moubaraki, B.; Abrahams, B. F.; Murray, K. S. *Aust. J. Chem.* **2014**, *67*, 1581–1587. (c) Rinck, J.; Novitchi, G.; Van den Heuvel, W.; Ungur, L.; Lan, Y.; Wernsdorfer, W.; Anson, C. E.; Chibotaru, L. F.; Powell, A. K. *Angew. Chem., Int. Ed.* **2010**, *49*, 7583–7587. (d) Blacque, O.; Amjad, A.; Caneschi, A.; Sorace, L.; Car, P. E. *New J. Chem.* **2016**, *40*, 3571–3577. (e) Li, Z. Y.; Wang, X.-Q.; Zhang, J.-J.; Liu, S.-Q.; Ni, J.; Sun, Y.-Ji. *Eur. J. Inorg. Chem.* **2015**, *2015*, 5702–5707.
- (11) (a) Papatriantafyllopoulou, C.; Wernsdorfer, W.; Abboud, K. A.; Christou, G. *Inorg. Chem.* **2011**, *50*, 421–423. (b) Stamatatos, T. C.; Teat, S. J.; Wernsdorfer, W.; Christou, G. *Angew. Chem., Int. Ed.* **2009**, *48*, 521–524. (c) Mereacre, V. M.; Ako, A. M.; Clérac, R.; Wernsdorfer, W.; Filoti, G.; Bartolome, J.; Anson, C. E.; Powell, A. K. *J. Am. Chem. Soc.* **2007**, *129*, 9248–9249. (d) Zaleski, C. M.; Depperman, E. C.; Kampf, J. W.; Kirk, M. L.; Pecoraro, V. L. *Angew. Chem., Int. Ed.* **2004**, *43*, 3912–3914. (e) Li, M.; Ako, A. M.; Lan, Y.; Wernsdorfer, W.; Buth, G.; Anson, C. E.; Powell, A. K.; Wang, Z.; Gao, S. *Dalton Trans.* **2010**, *39*, 3375–3377. (f) Schmitz, S.; van Leusen, J.; Ellern, A.; Kögerler, P.; Monakhov, K. Yu. *Inorg. Chem. Front.* **2015**, *2*, 1095–1100. (g) Bag, P.; Chakraborty, A.; Rogez, G.; Chandrasekhar, V. *Inorg. Chem.* **2014**, *53*, 6524–6533.
- (12) (a) Schray, D.; Abbas, G.; Lan, Y.; Mereacre, V.; Sundt, A.; Dreiser, J.; Waldmann, O.; Kostakis, G. E.; Anson, C. E.; Powell, A. K. *Angew. Chem., Int. Ed.* **2010**, *49*, 5185–5188. (b) Schmidt, S.; Prodius, D.; Mereacre, V.; Kostakis, G. E.; Powell, A. K. *Chem. Commun.* **2013**, *49*, 1696–1698. (c) Akhtar, M. N.; Mereacre, V.; Novitchi, G.; Tuchagues, J.-P.; Anson, C. E.; Powell, A. K. *Chem. - Eur. J.* **2009**, *15*, 7278–7282. (d) Stoian, S. A.; Paraschiv, C.; Kiritsakas, N.; Lloret, F.; Münck, E.; Bominaar, E. L.; Andruh, M. *Inorg. Chem.* **2010**, *49*, 3387–3401. (e) Nayak, S.; Roubeau, O.; Teat, S. J.; Beavers, C. M.; Gamez, P.; Reedijk, J. *Inorg. Chem.* **2009**, *48*, 216–221. (f) Chen, S.; Mereacre, V.; Anson, C. E.; Powell, A. K. *Dalton Trans.* **2016**, *45*, 98–106.
- (13) (a) Chandrasekhar, V.; Pandian, B. M.; Vittal, J. J.; Clérac, R. *Inorg. Chem.* **2009**, *48*, 1148–1157. (b) Chandrasekhar, V.; Pandian, B. M.; Azhakar, R.; Vittal, J. J.; Clérac, R. *Inorg. Chem.* **2007**, *46*, 5140–5142. (c) Sopsis, G. J.; Orfanoudaki, M.; Zampas, P.; Philippidis, A.; Siczek, M.; Lis, T.; O'Brien, J. R.; Milios, C. J. *Inorg. Chem.* **2012**, *51*, 1170–1179. (d) Liu, Y.; Chen, Z.; Ren, J.; Zhao, X. Q.; Cheng, Zhao, B. *Inorg. Chem.* **2012**, *51*, 7433–7435. (e) Zheng, Y.-Z.; Evangelisti, M.; Winpenny, R. E. P. *Chem. Sci.* **2011**, *2*, 99–102. (f) Yamaguchi, T.; Costes, J. P.; Kishima, Y.; Kojima, M.; Sunatsuki, Y.; Brefuel, T.; Vendier, L.; Wernsdorfer, W.; Tuchagues, J.-P. *Inorg. Chem.* **2010**, *49*, 9125–9135. (g) Alexandropoulos, D. I.; Cunha-Silva, L. C.; Lorusso, G.; Evangelisti, M.; Tang, J.; Stamatatos, T. C. *Chem. Commun.* **2016**, *52*, 1693–1696. (h) Dolai, M.; Ali, M.; Titiš, J.; Boča, R. *Dalton Trans.* **2015**, *44*, 13242–13249.
- (14) (a) Osa, S.; Kido, T.; Matsumoto, N.; Re, N.; Pochaba, A.; Mrozinski, J. *J. Am. Chem. Soc.* **2004**, *126*, 420–421. (b) Novitchi, G.; Wernsdorfer, W.; Chibotaru, L. F.; Costes, J. P.; Anson, C. E.; Powell, A. K. *Angew. Chem., Int. Ed.* **2009**, *48*, 1614–1647. (c) Feltham, H. L. C.; Clérac, R.; Powell, A. K.; Brooker, S. *Inorg. Chem.* **2011**, *50*, 4232–4234. (d) Baskar, V.; Gopal, K.; Helliwell, M.; Tuna, F.; Wernsdorfer, W.; Winpenny, R. E. P. *Dalton Trans.* **2010**, *39*, 4747–4750. (e) Chandrasekhar, V.; Dey, A.; Das, S.; Rouzières, M.; Clérac, R. *Inorg. Chem.* **2013**, *52*, 2588. (f) Novitchi, G.; Pilet, G.; Ungur, L.; Moshchalkov, V. V.; Wernsdorfer, W.; Chibotaru, L. F.; Luneau, D.; Powell, A. K. *Chem. Sci.* **2012**, *3*, 1169–1176. (g) Feltham, H. L. C.; Clérac, R.; Ungur, L.; Chibotaru, L. F.; Powell, A. K.; Brooker, S. *Inorg. Chem.* **2013**, *52*, 3236–3240. (h) Modak, R.; Sikdar, Y.; Cosquer, G.; Chatterjee, S.; Yamashita, M.; Goswami, S. *Inorg. Chem.* **2016**, *55*, 691–699. (i) Ida, Y.; Ghosh, S.; Ghosh, A.; Nojiri, H.; Ishida, T. *Inorg. Chem.* **2015**, *54*, 9543–9555.
- (15) (a) Chandrasekhar, V.; Pandian, B. M.; Boomishankar, R.; Steiner, A.; Vittal, J. J.; Houri, A.; Clerac, R. *Inorg. Chem.* **2008**, *47*, 4918–4929. (b) Chandrasekhar, V.; Bag, P.; Kroener, W.; Gieb, K.; Müller, P. *Inorg. Chem.* **2013**, *52*, 13078–13086. (c) Das, S.; Hossain, S.; Dey, A.; Biswas, S.; Pardo, E.; Lloret, F.; Chandrasekhar, V. *Eur. J. Inorg. Chem.* **2014**, *2014*, 3393–3400. (d) Goura, J.; Guillaume, R.; Rivière, E.; Chandrasekhar, V. *Inorg. Chem.* **2014**, *53*, 7815–7823. (e) Biswas, S.; Das, S.; van Leusen, J.; Kögerler, P.; Chandrasekhar, V. *Dalton Trans.* **2015**, *44*, 19282–19293.
- (16) (a) Biswas, S.; Das, S.; van Leusen, J. V.; Kögerler, P.; Chandrasekhar, V. *Eur. J. Inorg. Chem.* **2014**, *25*, 4159–4167.

- (18) (a) *Vogel's Textbook of Practical Organic Chemistry*, 5th ed.; Furniss, B. S., Hannaford, A. J., Smith, P. W. G., Tatchell, A. R., Eds.; ELBS and Longman: London, 1989. (b) Williams, D. B. G.; Lawton, M. J. *Org. Chem.* **2010**, *75*, 8351–8354. (c) Zeng, X.; Coqui re, D.; Alenda, A.; Garrier, E.; Prang e, T.; Li, Y.; Reinaud, O.; Jabin, I. *Chem. - Eur. J.* **2006**, *12*, 6393–6402.
- (19) (a) SMART & SAINT Software Reference Manuals, version 6.45; Bruker Analytical X-ray Systems, Inc.: Madison, WI, 2003. (b) Sheldrick, G. M. SADABS, version 2.05; University of G ttingen: G ttingen, Germany, 2002. (c) SHELXTL Reference Manual, ver. 6.1; Bruker Analytical X-ray Systems, Inc.: Madison, WI, 2000. (d) Sheldrick, G. M. SHELXTL, version 6.12; Bruker AXS Inc.: WI, Madison, 2001. (e) Sheldrick, G. M. *Acta Crystallogr., Sect. A: Found. Crystallogr.* **2008**, *64*, 112–122. (f) Dolomanov, O. V.; Bourhis, L. J.; Gildea, R. J.; Howard, J. A. K.; Puschmann, H. *J. Appl. Crystallogr.* **2009**, *42*, 339–341. (g) Bradenburg, K. *Diamond*, Ver. 3.1eM; Crystal Impact GbR: Bonn, Germany, 2005.
- (20) (a) Zheng, Y.-Z.; Lan, Y.; Anson, C. E.; Powell, A. K. *Inorg. Chem.* **2008**, *47*, 10813–10815. (b) Guo, P.-H.; Liu, J.-L.; Zhang, Z.-M.; Ungur, L.; Chibotaru, L. F.; Leng, J.-D.; Guo, F. S.; Tong, M.-L. *Inorg. Chem.* **2012**, *51*, 1233–1235. (c) Abbas, G.; Lan, Y.; Kostakis, G. E.; Wernsdorfer, W.; Anson, C. E.; Powell, A. K. *Inorg. Chem.* **2010**, *49*, 8067–8072. (d) Lin, P.-H.; Burchell, T. J.; Ungur, L.; Chibotaru, L. F.; Wernsdorfer, W.; Murugesu, M. *Angew. Chem., Int. Ed.* **2009**, *48*, 9489–9492. (e) Yan, F. P.; Lin, P.-H.; Habib, F.; Aharen, T.; Murugesu, M.; Deng, Z.-P.; Li, G.-M.; Sun, W.-B. *Inorg. Chem.* **2011**, *50*, 7059–7065. (f) Zhao, L.; Wu, J.; Ke, H.; Tang, J. *Inorg. Chem.* **2014**, *53*, 3519–3525.
- (21) (a) Liu, W.; Thorp, H. H. *Inorg. Chem.* **1993**, *32*, 4102–4105. (b) Brown, I. D.; Wu, K. K. *Acta Crystallogr., Sect. B: Struct. Crystallogr. Cryst. Chem.* **1976**, *32*, 1957–1959.
- (22) (a) Xue, S.; Zhao, L.; Guo, Y.-N.; Tang, J. *Dalton Trans.* **2012**, *41*, 351–353. (b) Randell, N. M.; Anwar, M. U.; Drover, M. W.; Dawe, L. N.; Thompson, L. K. *Inorg. Chem.* **2013**, *52*, 6731–6742. (c) Anwar, M. U.; Thompson, L. K.; Dawe, L. N.; Habib, F.; Murugesu, M. *Chem. Commun.* **2012**, *48*, 4576–4578.
- (23) (a) Sorace, L.; Benelli, C.; Gatteschi, D. *Chem. Soc. Rev.* **2011**, *40*, 3092–3104. (b) Aldamen, M. A.; Cardona-Serra, S. C.; Clemente-Juan, J. M. C.; Coronado, E.; Gaita-Ari o, A. G.; Mart -Gastaldo, C. M.; Luis, F.; Montero, O. *Inorg. Chem.* **2009**, *48*, 3467–3479.
- (24) (a) Zheng, Y.-Z.; Lan, Y.; Anson, C. E.; Powell, A. K. *Inorg. Chem.* **2008**, *47*, 10813–10815. (b) Xue, S.; Zhao, L.; Guo, Y.-N.; Deng, R.; Guo, Y.; Tang, J. *Dalton Trans.* **2011**, *40*, 8347. (c) Guo, P.-H.; Liu, J.-L.; Zhang, Z.-M.; Ungur, L.; Chibotaru, L. F.; Leng, J.-D.; Guo, F.-S.; Tong, M.-L. *Inorg. Chem.* **2012**, *51*, 1233–1235. (d) Langley, S. K.; Chilton, N.; Gass, I. A.; Moubaraki, B.; Murray, K. S. *Dalton Trans.* **2011**, *40*, 12656–12659.
- (25) Pasatoiu, T. D.; Ghirri, A.; Madalan, A. M.; Affronte, M.; Andruh, M. *Dalton Trans.* **2014**, *43*, 9136.
- (26) Upadhyay, A.; Das, C.; Langley, S. K.; Murray, K. S.; Srivastava, A. K.; Shanmugam, M. *Dalton Trans.* **2016**, *45*, 3616–3626.
- (27) Rinehart, J. D.; Long, J. R. *Chem. Sci.* **2011**, *2*, 2078–2085.
- (28) Blundell, S. J. *Magnetism in Condensed Matter*; Oxford University Press: Oxford, 2012.
- (29) Singh, S. K.; Tibrewal, N. K.; Rajaraman, G. *Dalton Trans.* **2011**, *40*, 10897–10906.
- (30) Goura, J.; Brambleby, J.; Goddard, P.; Chandrasekhar, V. *Chem. - Eur. J.* **2015**, *21*, 4926–4930.
- (31) Woodruff, D. N.; Tuna, F.; Bodensteiner, M.; Winpenny, R. E. P.; Layfield, R. A. *Organometallics* **2013**, *32*, 1224–1229.
- (32) Huang, W.; Xu, J.; Wu, D.; Huang, X.; Jiang, J. *New J. Chem.* **2015**, *39*, 8650–8657.
- (33) Landee, C. P.; Mudgett, D. M.; Foxman, B. M. *Inorg. Chim. Acta* **1991**, *186*, 45–49.
- (34) Gatteschi, D.; Sessoli, R.; Villain, J. *Molecular Nanomagnets*; Oxford University Press: Oxford, 2011.
- (35) Goura, J.; Brambleby, J.; Topping, C. V.; Goddard, P. A.; Suriya Narayanan, R.; Bar, A. K.; Chandrasekhar, V. *Dalton Trans.* **2016**, *45*, 9235–9249.
- (36) Blundell, S. J.; Pratt, F. L. *J. Phys.: Condens. Matter* **2004**, *16*, R771–R828.
- (37) Gatteschi, D.; Sessoli, R. *Angew. Chem., Int. Ed.* **2003**, *42*, 268–297.
- (38) Christou, G.; Gatteschi, D.; Hendrickson, D. N.; Sessoli, R. *MRS Bull.* **2000**, *25*, 66–71.
- (39) Lin, P.-H.; Burchell, T. J.; Ungur, L.; Chibotaru, L. F.; Wernsdorfer, W.; Murugesu, M. *Angew. Chem., Int. Ed.* **2009**, *48*, 9489–9492.
- (40) Miklovi , J.; Valigura, D.; Bo a, R.; Titi , J. *Dalton Trans.* **2015**, *44*, 12484–12487.
- (41) Jiang, S.-D.; Wang, B.-W.; Sun, H.-L.; Wang, Z.-M.; Gao, S. J. *Am. Chem. Soc.* **2011**, *133*, 4730–4733.